ECN-C--05-064

Final report of the Annexlyse project

Analysis of aerodynamic field measurements on wind turbines

Schepers, J.G.

(ECN)

van Rooij, R.P.J.O.M.

(Delft University of Technology)

JUNE 2005

Acknowledgement/Preface

The research described in this report is partly funded by SenterNovem B.V. project number 2020-01-13-10-003. Additional funding for ECN's contribution was obtained from the 'Samenwerkingsfinanciering' program (project 7.4154).

The authors would like to express their gratitude to Maureen Hand (National Renewable Energy Laboratory, USA) Helge Aagaard Madsen (RISØ National Laboratory, Denmark) and Takao Maeda (Mie University, Japan) for their support in understanding the data contained in this report.

Abstract

In this report the most important results from the Annexlyse project are summarized. Annexlyse is a project carried out by the Energy Research Center of the Netherlands, ECN and the Delft University of Technology DUT. It's objective was to carry out a thorough analysis of the aerodynamic field measurements which have been taken in two IEA Annexes:

- IEA Annex XIV: Field rotor aerodynamics
- IEA Annex XVIII: Enhanced Field Rotor Aerodynamics Database

Contents

List of tables

List of figures

Summary

In this report the most important results of the Annexlyse project are summarized. This project was carried out by the Energy research Center of the Netherlands, ECN and the Delft University of Technology, DUT in the period from May 2002 until December 2004.
It was sponsored by the Dutch Agency for Energy and the Environment, Novem.
The objective of the Annexlyse project was to perform a thorough analysis of the aerodynamic field measurements which were collected in two IEA Annexes:

- IEA Annex XIV: Field rotor aerodynamics
- IEA Annex XVIII: Enhanced Field Rotor Aerodynamics Database

In these Annexes the pressure distributions are measured on various facilities at different radial positions. These pressure distributions are integrated to the aerodynamic normal and tangential forces.

In the project a number of activities have been performed which focused on the measurements itself, the validation of aerodynamic (and aero-elastic) models and the improvement of aero-elastic models. The activities are summarized in the present report but for more details reference is made to various task reports, papers and journal articles.
Important subjects which have been addressed are measurement uncertainties, the problems associated with the angle of attack, and the validation and improvement of aero-elastic models,
The relation between local aerodynamic loads and the global blade and rotor loads (which are of direct importance for designers) is also considered.

The main conclusion from the Annexlyse project should be that, despite all measurement uncertainties, the character of the IEA Annex XIV/XVIII measurements is so much unique that they clearly contributed to the development and validation of aerodynamic models indeed. This holds among others for 3D stall models, tip models and yaw models. It was shown that the behaviour of blade and rotor loads can only be understood from measurements of the underlying sectional loads, as provided in this project. Thereto it should be realised that local aerodynamic effects like tip effects, rotational effects, the variation in induced velocity at yaw etc. were all shown to contribute significantly (in the order of 10% or more) to the overall blade and rotor loads. Additionally it was found that differences between calculated and measured blade and rotor loads (as found from conventional wind turbine validation programs, like the European Union JOULE III project Verification of European Wind Turbine Codes, (Schepers, 2001)) can have a very complicated origin and may even be caused by 'compensating errors'. Finally the fact that measurements on more than one wind turbine could be used, clearly led to a much more general validation of aerodynamic models where trends and dependencies on model parameters (i.e. blade layout, twist etc) could be confirmed, investigated and/or discovered.

1. Introduction

In this report the most important results of the Annexlyse project are summarized. This project was carried out by the Energy Research Center of the Netherlands, ECN and the Delft University of Technology, DUT in the period from May 2002 until December 2005.
It was sponsored by the Dutch Agency for Energy and the Environment, Novem.
The objective of the Annexlyse project was to perform a thorough analysis of aerodynamic field measurements in order to improve and validate aerodynamic models.
The measurements considered are of a special character in the sense that not only global blade and shaft loads are measured (which is common in measurement programs on wind turbines), but also local aerodynamic properties at different span wise locations along a wind turbine blade. This includes the measurements of pressure distributions and the associated local aerodynamic forces (normal and tangential to the chord) and inflow data. The aerodynamic measurements have been obtained from test programs on different wind turbines and they originate from the database which was created in two IEA Annexes, coordinated by ECN:

- IEA Annex XIV: Field Rotor Aerodynamics, and its successor project:
- IEA Annex XVIII: Enhanced Field Rotor Aerodynamics Database

IEA Annex XIV started in 1991 and ended in 1997. It's successor project, IEA Annex XVIII ran from 1997 to 2001.
In IEA Annex XIV, a total of five full scale aerodynamic test programs were coordinated. These programs were carried out by:

- Delft University of Technology, DUT Netherlands;
- Netherlands Energy Research Foundation, ECN, Netherlands;
- National Renewable Energy Laboratory, NREL, USA.
- RISØ the test station for Wind Turbines, Dk;
- Imperial College, IC and Rutherford Appleton Laboratory, RAL, United Kingdom;

In IEA Annex XVIII the same institutes as mentioned above participated, however without Imperial College, IC and Rutherford Appleton Laboratory, RAL. In addition the following institutes participated:

- Mie University; Japan
- Centre of Renewable Energy Systems, CRES, Greece

The database of the IEA Annexes can be found on the Internet http://www.ecn.nl/wind/other/IEA/index.en.html). The final reports of the IEA Annexes which include a description of the database and the experimental facilities are given in (Schepers et al, 1997; Schepers et al, 2002)

Hence the objective of the Annexlyse project, described in the present report, was to analyse the aerodynamic field measurements from the IEA Annex XIV/XVIII database. Thereto the present report summarizes the measurement facilities and the database in the sections 2 and 3. This is followed by a summary of the most important activities which are performed in the Annexlyse project. These activities are (with task numbers from the work plan which has been submitted to Novem in December 2001):

- An inventory of previous analyses on the IEA Annex XIV/XVIII data (usually by other parties than the Annexlyse participants). The information from these previous analyses facilitated and guided the analyses of the present project. The activities were part of task 1 in the Annexlyse work plan and they are summarized in section 4;

- A consistency check on the measurements. Thereto the relation between the local aerodynamic loads and the overall rotor(blade) loads is determined. To this end the overall rotor loads are calculated by integrating the measured segment loads along the span and the resulting loads are compared with the directly measured loads from strain gauges. These activities are part of task 2 of the Annexlyse work plan (a selection of the most suitable campaigns) but they are also part of task 3.4 in which the relation between local aerodynamic loads and global rotor loads is assessed. The activities are summarized in section 5.
- An analysis of the angle of attack: The angle of attack is a crucial quantity in analysing aerodynamic field measurements. Different methods to derive the angle of attack have been developed. They are reported in section 6. The activities were part of task 3.1 of the Annexlyse project.
- An evaluation of the measured aerodynamic characteristics (normal and tangential force coefficients as function of angle of attack) on 3D effects. To this end the measured characteristics are compared with results from different aerodynamic 3D models. These activities were part of task 3.2 of the Annexlyse project. They are reported in section 7.
- An evaluation of the measured time series at (more or less) non-yawed conditions. Thereto the results of an aero-elastic code are used. On basis of this comparison, the parameters in 3D models have been tuned. The results obtained with the newly tuned 3D models have also been compared with the measurements. These activities were part of task 3.4 and task 4 of the Annexlyse work plan. They are described in section 8 an 9;
- An evaluation of the azimuthally binned averaged normal forces at yawed conditions. In this analysis, emphasis is put on the variation of the induced velocity over the rotor-plane which effects the yawing stability. These activities were part of the task 3.4 of the Annexlyse project and they are reported in section 10.

The present report only gives a global summary of the most important results. For background information on the different tasks, reference is made to task reports which are stored on the Annexlyse Internet site, and to the papers and journal articles which have been prepared on the project, in particular (van Rooij, 2003a; van Rooij, 2003b; van Rooij 2005; Schepers, 2003a; Schepers 2004a; Schepers, 2004e).

2. Description of facilities

As mentioned in the previous section, the measurements which have been used in this project, originate from the database created in IEA Annex XIV and IEA Annex XVIII. In these annexes measurements became available on facilities from the following institutes:

- Delft University of Technology, DUT, The Netherlands: The DUT experiments are carried out on a 2 bladed, 10 m diameter turbine, see figure 2.1. The blades are untwisted and untapered. One of the blades is instrumented with pressure taps at 4 radial positions. The inflow conditions are measured at 1 radial positions with a pitot/3hole probe.
- Netherlands Energy Research Foundation, ECN, Netherlands. The ECN experiments are carried out on a 2 bladed, 27.4 m diameter turbine, see figure 2.2. The blades are twisted and tapered. One of the blades is instrumented with pressure taps at 3 radial positions. The inflow conditions are measured at 1 radial position with a five hole pitot probe.

Figure 2.1: *DUT facility*

Figure 2.2: *ECN facility*

- National Renewable Energy Laboratory, NREL, USA: The NREL experiments were carried out on a 2 bladed, 10 m diameter turbine, see figure 2.3. The rotor has been equipped with different blades. Within the present IEA Annexes, measurements on two types of blades have been supplied:
  - An untwisted and untapered blade;
  - A similar blade, without taper, but with twist.

  The blade is instrumented with pressure taps at 4 radial positions for the untwisted untapered blade and 5 radial positions for the twisted blade. The inflow conditions are measured either with a pitot probe in combination with a wind vane, or with a five hole pitot probe. The measurements on the untwisted untapered blade are identified as Phase II, the measurements on the untapered twisted blade are identified as Phase III or Phase IV where Phase IV denotes measurements with a pitot probe and Phase III denotes the measurements with a wind vane.

Figure 2.3: *NREL facility*

- RISØ National Laboratory, Denmark: The RISØ experiments were carried out on a 3 bladed, 19 m diameter turbine, see figure 2.4. The blades are twisted and tapered. RISØ was the only party in the IEA Annexes, which measures the aerodynamic forces by means of force balances, instead of pressure taps. Thereto one of the blades is instrumented at 3 radial positions. The inflow conditions are measured at 1 radial position with a five hole pitot probe.

Figure 2.4: *RISØ test facility*

- Mie University, Japan: The Mie University experiments were carried out on a 3 bladed turbine, see figure 2.5. The blades are twisted and tapered. One of the blades is instrumented with pressure taps at 4 radial positions. The inflow conditions are measured at 2 radial positions with a five hole pitot probe.

Figure 2.5: *Mie test facility*

- Imperial College, IC and Rutherford Appleton Laboratory, RAL, United Kingdom: The IC/RAL experiments were carried out on a 3 bladed, 16.9 m diameter turbine. The blades are twisted and tapered.

A summary of the rotor details is given in table 1.

Table 1: Rotor details.

Geometry	**ECN**	**DUT**	**NREL**	**MIE**	**RISØ**
Designation	Aerpac 25 WPX			Aerpac APX-40	LM 8.2
Number of blades	2	2	3	3	3
Rotor diameter	27.66m	10.0m	10.06m	10.0m	19.0m
Cone	5. deg.	No	3.41 deg.	No	No
Tilt	5. deg.	No	No	No	5. deg.
Taper	Yes	No	No	Yes	Yes
Twist	12 deg.	No	Phase III-IV Twisted At r/R=.25, 30 deg	12 deg.	15 deg
Pitch	Adjustable	Adjustable	Adjustable	Adjustable	Approx. -1.8^{o}

Airfoil series	NACA 44xx	NLF(1)-0416	S809	DU 91-W2-250 DU 93-W-210 NACA 63-618	NACA 63-2xx
Thickness Root-Tip	26% - 16%	16%	20.95%	25% - 18%	24.5% - 17.5%
Start aerodynamic blade part	28%	20%	14%	27%	27%
Tower	Pile	Pile	Pile	Pile	Lattice
Hub height	22.4m	15.3m	17.03m	13.3m	29.3m
Remarks	Up-wind turbine	Up-wind turbine	Mainly Down-wind Free yaw	Up-wind turbine	Up-wind turbine

The structural properties of the turbines are given in (Schepers,1997; Schepers-2001)

The measurements focussed on environmental properties and the aerodynamic rotor performance. The environmental parameters of concern are the wind speed and directions, wind shear and some additional properties like barometric pressure and temperature to e.g. derive the air density. The task report 2 (van Rooij, 2004) gives detail information about this.

The measurements devices for obtaining the aerodynamic properties are located mainly at the blade. Some are at the root others along the span. An overview is given in table 2. The differences between the configurations are substantial in particular wrt the flow probe devices. This obviously complicates a proper comparison of the facilities

Table 2: Overview of equipment and its location at the blade.

Experimental Set-up	**ECN**	**DUT**	**NREL**	**MIE**	**RISØ**
Tap stations					
Pressure orifices	47 taps D= 1.mm	59 taps and when 2 segments 28 taps D= 0.4mm	28 taps at Phase II 22 taps Phase III-IV D= 1.mm	60 taps D= 0.4mm	**Not applicable.** Segment force measurements
Radial locations r/R	36.0% 64.0% 82.0%	30.0% 50.0% 70.0% 90.0%	30.0% 47.0% 63.0% 80.0% 95.0%	32.5% 50.0% 70.0% 90.0%	Ave. 37.4% Ave. 68.2% Tip
Radial locations c/r	.284 .112 .062	.333 .200 .143 .111	.305 .195 .145 .113 .100	.252 .118 .06 .031	
Distributed	Constant span	Staggered	Constant span	Constant span	N/A
Remarks	Simultaneously	Mostly individually	Simultaneously	Individually	Simultaneously
Flow probe					
Flow probe, type, length, diameter	Sphere, 5 hole L= .82c D= 58mm	3 hole L= 0.55c D= 10mm 5(6) hole L= .12c D= 5mm	Phase II Flag, Phase III Flag, Phase iV 5 hole L= .81c D= 6.3mm	Sphere, 5 hole L= 1.0c	5 hole
Angle flow probe with chord	- 14.deg.	0.deg.	-20.deg.	0.deg.	
Distance from tap stations	Probe fixed at 42% span	ca. 6%	ca. 4%	6% and approx. 12%	Probe fixed at 50% span
Q-probes	At 42%, not applied	3 Kiel probes at 3 of the 4 positions: 36% 56% 76% 96%		Two 5-hole probes	
Electronic pressure sensors	Scanivalve ZOC23	PSI-ESP	PSI-ESP	Scanivalve ZOC	
Data rate for all pressures*	128 Hz	333 Hz		95 Hz	

Averaged (azimuth angle)	every 4 deg. at 40 rpm	every 6 deg. azimuth	every 8 deg. at 72rpm		
Radial location of sensors**	33,4% 60.6% 75.8%	86%	Close to pressure taps		
Tubes to sensors; length and diameter	L = 1.1m D= 1 mm	L = 0.60m D = 2 mm Subsequently L= 0.30m D= 1 mm			
Reference pressure	Hub static	Hub static (Hub pitot)	Hub static	Hub static	
Strain gauges					
Direction	Edgewise Flap	Edgewise Flap	Edgewise Flap		
Radial location	10%	Root	Root and 8%,25%, 60% Phase III-IV		
Accelerometers			Tip		
Miscellaneous					
Data transfer Via sliprings	Analogue	Analogue, Digital(1996)			

Note that Imperial College, IC (and Rutherford Appleton Laboratory) and CRES are not mentioned in table 1 and 2. The program of the first partner was not really suited for a realistic comparison due to many problems during the measurements. The CRES test program was delayed and unfortunately no measurements could be supplied within the IEA Annex XIV/XVIII.

3. Description of the IEA Annex XIV/XVIII database

In IEA Annex XIV/XVIII a joint measurement program was agreed upon in order to create the database. The measurements have been supplied in the following form:

- Time series. Time series at non-yawed conditions and at yawed conditions are supplied. The angle of attack ranges from negative values to deep stall values. Time series at stand still have also been provided;
- Sectional profile coefficients (c_n, c_t, c_m) under rotating conditions. If available, the 2D wind tunnel sectional profile coefficients have also been supplied.

In June 2001, the following measurements were stored into the database:

- ECN: 54 campaigns with a length of about 1 minute each (Note that all pressure taps stations are measured simultaneously);
- NREL: 40 campaigns with a length of approximately 1 minute each. Note that all pressure taps stations are measured simultaneously;
- RISO: 8 campaigns, with a length of 10 minutes each. Note that all force balance stations are measured simultaneously;
- DUT: 300 campaigns with a length of approximately 1 minute each. Note that the pressure tap stations are measured separately;
- Mie University: 12 campaigns with a length of approximately 1 minute each. Note that the pressure tap stations are measured separately;
- IC/RAL: 1 Campaign with a length of approximately 1 minute.

The data file formats and the conventions have been harmonized in order to make the database easily accessible.

The database is accessible on CD-ROM but also on an Internet site:
http://www.ecn.nl/unit_de/wind/annexxiv/index.html
In principle, the database is freely available for third parties. However access is only granted if the receiving party agrees (on basis of a Gentleman's or Lady's Agreement) that the IEA Annex XIV/XVIII participants will be informed on the experiences which have been gained with the database. This feedback from the users of the database turned out to be extremely useful, because the quality of the database could be improved on basis of recommendations given by the users, see section 4.

A spreadsheet file has been created withing the Annexlyse project which is added to the database and which gives an overview of the specific configuration details. This facilitates the selection within the database.

4. Inventory of previous analyses on IEA Annex XIV/XVIII data

As explained in section 3, the IEA Annex XIV/XVIII database is freely available to third parties on the condition that the IEA Annex XVIII participants (including DUT and ECN) are informed on the experiences with it. A limited number of database users had already performed analyses on the aerodynamic measurements before the Annexlyse project had started. These, already existing, analyses have been summarized in task 1 of the Annexlyse project.
In this way an overlap between the Annexlyse activities and the work already performed could be avoided. Furthermore, the already existing analyses guided and facilitated the analyses which ECN and DUT intended to carry out.
The results of this task are reported in (Schepers, 2003a; Schepers 2003b). The main conclusions and recommendations are given below.

Conclusions
The main conclusions, which were drawn from the inventory of analyses on the Annex XVIII data are:

- Aerodynamic field measurements are difficult to use for a detailed validation of dynamic stall models. A more global validation of dynamic stall models on basis of statistical data was believed to be possible;
- The most successful activities on the IEA Annex XIV/XVIII data have been:
  - Comparison of rotating (mean) airfoil data with 2D airfoil data. Several differences are found, among others the well known stall delay at the inner sections, i.e. the aerodynamic lift forces are considerable higher compared to 2D wind tunnel experiments;.
  - Validation of CFD codes (RANS codes, free wake panel methods and RFOIL) on basis of pressure distributions. It must be noted that little validation of blade element momentum methods is reported;
  - Validation of yaw models on basis of azimuthally binned averaged normal forces and inflow data (i.e. angles of attack);
- The IEA Annex XIV/XVIII measurements have mainly been used for validation of existing models. Development of new aerodynamic models on basis of the measurements has hardly been reported;
- Most comparisons between calculations and measurements show a good to reasonable agreement below stall, but above stall the agreement becomes poor.

Uncertainties
The main uncertainties in the interpretation of the measurements are associated to the angle of attack, the dynamic pressure and the fact that the incoming inflow conditions are non-stationary and partly unknown. To some extent the latter problem is overcome by selecting data according to a baseline criterion as NREL did (measurements at relatively stable conditions are selected). Obviously the measurements, which recently have been taken by NREL in the wind tunnel (the well known NASA Ames experiment) donot suffer from these uncertainties in the inflow.

Despite considerable improvement s and corrections to cope with errors or anomalies in the pressure system, the set-ups still have some draw-backs and some uncertainties, which are inherent to these kind of experiments.

For validation of some CFD methods the modelling of laminar-turbulent transition turns out to be a problem. Unfortunately no experiments with fixed transition are included in the IEA Annex XIV/XVIII database.
When comparing calculations with measured results, another very important uncertainty was found in the fact that the model descriptions of the IEA Annex XIV/XVIII facilities (i.e. the geometric data, the mass and stiffness data etc) were not always complete. Hence differences

between calculations and measurements may be a result of uncertainties in the aero-elastic model descriptions.

Recommendations from previous analyses

For the remaining Annexlyse tasks it was recommended to:

- Investigate alternative definitions for the angle of attack, and try, where possible, to avoid the use of an angle of attack and the non-dimensionalisation with dynamic pressure. Thereto a comparison will be made on basis of dimensional values of the aerodynamic forces;
- Although a global validation of dynamic stall models on basis of statistical data (instead of chaotic dynamic stall loops) is believed to be possible it was decided to perform this task in IEA Annex XX, where the above mentioned NASA-Ames wind tunnel measurements are analysed. The stationary well known conditions in the wind tunnel will make the validation of dynamic stall models easier;
- Validate BEM models using the IEA Annex XIV/XVIII data;
- Derive, where possible, baseline data for all facilities, The baseline criteria as defined by NREL seem appropriate, although the inclusion of the time delay between the mast and turbine may give an improvement. For some facilities it is known that no proper indication of the inflow is available. Then it is recommended to define selection criteria from the turbine behaviour;
- Focus in the analyses on those IEA Annex XVIII facilities where also spanwise pressure distributions are available;
- Investigate the yaw behaviour for the turbines by binning c_n and the inflow quantities against azimuth angle. From this data, dependencies in the inflow distributions should be determined and thereafter an empirical formula for inflow variation in yaw should be studied. It is expected that the measurement unertainties play a limited role in such investigation, since it is mainly the variation of the aerodynamic quantities which is of importance instead of the absolute level.
- Hardly any investigations are performed on ‘stand-still’ aerodynamics, nor the correlation between the different measurement sections along the blade span has been investigated. It is recommended to include such investigations.

Almost all of these recommendations were followed in the remaining tasks of the project. The validation of the dynamic stall modelling and the analysis of stand still aerodynamics will be performed in a follow-up project, i.e. IEA Annex XX on basis of NREL's NASA-Ames wind tunnel measurements because the uncertainty in the inflow plays the largest role in these analysis.

5. Consistency check on measurements

For the ECN facility, rotor loads have been calculated by fitting a blade load distribution to the measured segment loads at different locations along the blade. The resulting rotor loads (in the sequel they are denoted as 'pressure' loads) are compared with the 'directly' measured loads, i.e. the loads measured from the strain gauges. This work is described in detail by Feigl (2003). It is part of task 2 of the project (see also the task report (van Rooij, 2004))

8 ECN campaigns are considered. The main difference between the campaigns was in the pitch angle, which ranged from +9.7 degrees in campaign 1 to –12.6 degrees in campaign 8.

The 'pressure' axial force and the 'pressure' torque are derived from a load distribution which is fitted to the measured segment forces, i.e. to the normal and tangential forces at the 3 instrumented stations at 30% span, 60% span and 80% span.
In the load distribution, the c_n's and c_t's are assumed to vary linearly between the instrumented sections and they drop linearly to zero towards the tip and the root.

A graphical comparison of the 'pressure' and 'direct' loads as function of time is given in the figures 5.1 and 5.2, where the campaigns are plotted in sequential order.

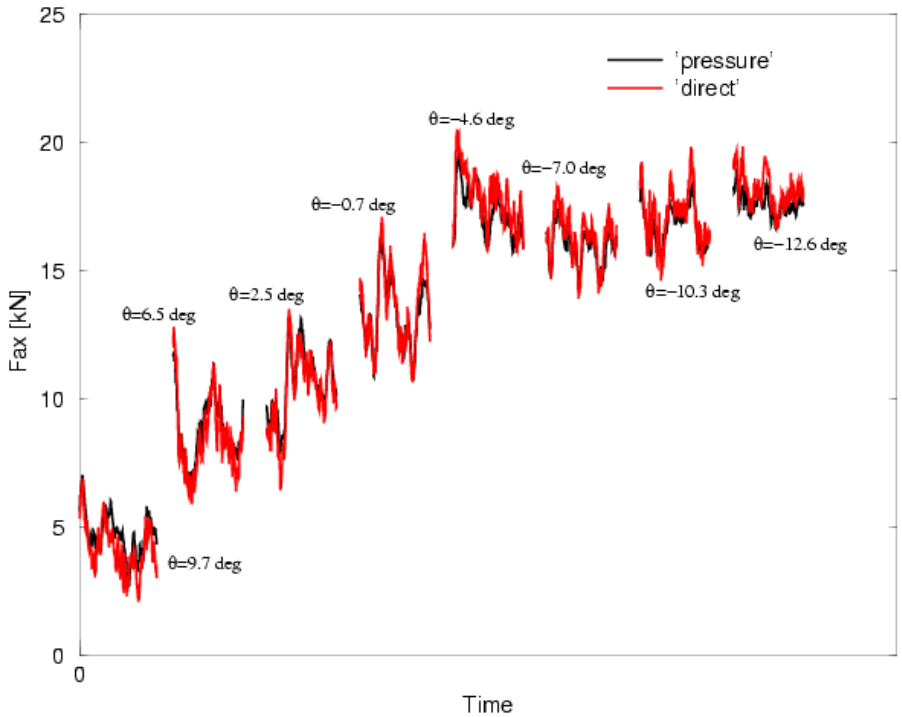

Figure 5.1: *ECN measurements: "Pressure" and "direct" axial force as function of time*

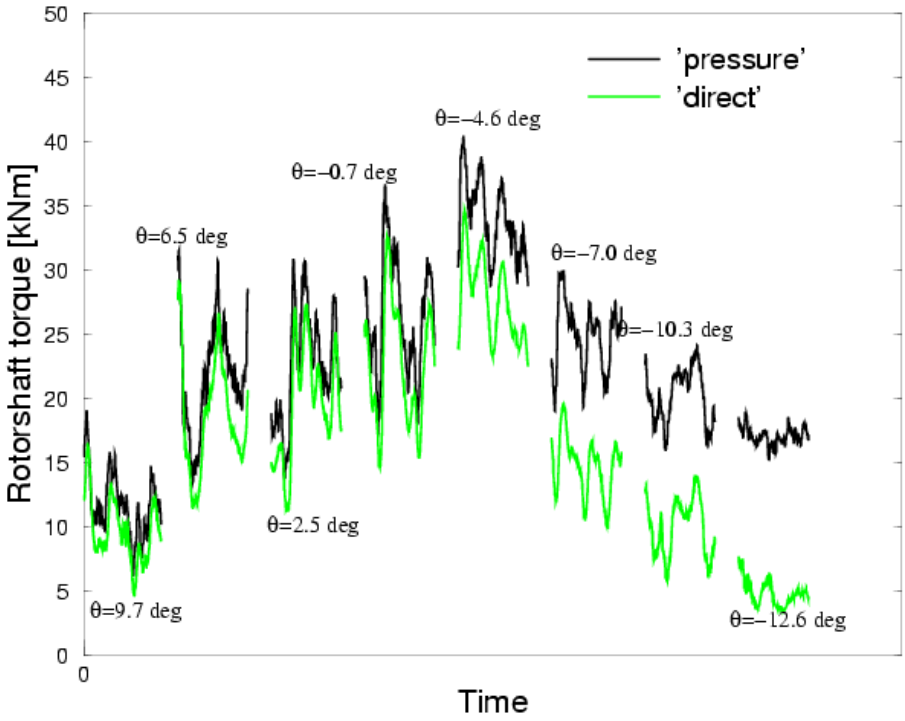

Figure 5.2: *ECN Measurements: 'Pressure' and 'direct' rotorshaft torque as function of time for 8 campaigns*

Figure 5.1 shows the agreement between 'pressure' and 'direct' axial force to be extremely well. This holds both for the agreement in terms of variations as well as the agreement in terms of level. This is a remarkable observation since the 'pressure' and 'direct' axial forces are obtained in very different ways. It shows that the measurement of axial force and normal force is reliable and it confirms the expectation that the axial force is accurately calculated if the aerodynamic segment forces are predicted and prescribed well.

In figure 5.2 the 'pressure' torque is compared with the 'direct' torque.
The agreement in 'shape' of the time series turns out to be very well except for campaign 8. The agreement in absolute levels gets poorer with increasing campaign number (i.e. with decreasing pitch angle and increasing angle of attack). It should be noted that the directly measured torque is believed to be reliable. This is among others confirmed by the fact that it compares very well with the torque derived from the measured generator power. As such it is the 'pressure' torque which is less reliable. Many explanations for the differences between the ' direct' and 'pressure torque' at decreasing pitch angles were investigated, see (Schepers, 2004a), but the final conclusion is that the differences have to be caused by the inaccuracy in tangential force. which is derived from the measured pressure distribution. Thereto it should be realised that the local tangential force is derived from integration of the pressure distribution and small errors in pressure tap positions (which are inevatible in view of the limited number of taps) and small errors in the surface direction will have a large effect on this quantity.
For the campaign at positive pitch angles the contribution of the tangential force to the torque is small compared to the contribution of the normal force, but its contribution increases with decreasing pitch angles. Hence the possible inaccuracy in measured tangential force plays the largest role at a pitch angle of –12.6 degrees.

It is noted that the tangential force hardly contributes to the axial force and as such the good agreement between 'pressure' and 'direct' axial force is possible.

Finally it is noted that the same observations are found in the NREL measurements from IEA Annex XIV/XVIII (where only the rotorshaft torque has been measured): For positive pitch angles (3 and 8 degrees) there is a good agreement between 'pressure' and 'direct' torque (differences in mean value are in the order of a few percents or even lower). For negative pitch angles the 'pressure' torque is much higher (at a pitch angle of -8.9 degrees, the 'pressure' torque is twice the 'direct' torque).

6. Angle of attack

A representative inflow angle is a major parameter for understanding the flow performances and is essential in comparison with 2D measurements and related stall models. On a rotating blade this parameter can never be obtained directly not even with so called flow devices like “flag” or “flow probe”. These devices are attached to the blade and obtain data in front of the airfoil. The local flow angle is therefore subject to the flow distortions caused by the lift and drag of blade and wake behind the rotor. The upflow angle has here by far the most important influence. The results from these flow devices are associated with the characteristics of the airfoil sections which are at a slightly different span location and in particular in the unsteady flow situation it can be subject to different dynamic flow behaviour as-well. In addition the dynamic behaviour of the measurement device itself can add uncertainties and probe readings could lead to misinterpretation.
Apart from these flow devices, the angle-of-attack (AOA) can be determined from pressure distributions or calculated from assumed flow geometries. The latter is an indirect method and is the most complicated technique. These methods also have drawbacks and it is difficult to establish the best angle-of-attack derivation.
Several options will be investigated and compared with each other to show the pro’s and con’s of the different methods. This should increase the reliability of the derived flow performance and should lead to better understanding of the flow behaviour.

During the years of field test experiments many methods to determine the angle-of-attack are applied and that is the reason why only an evaluation will be considered here. These techniques and the necessary corrections have generally been well documented already. In particular NREL and DUT were involved in the investigations. An overview of some methods with respect to field experiments are given in e.g. the final reports of the Annexes 14 and 18, chapter 5 and 6 respectively (Schepers et al, 1997) and (Schepers et al, 2002). The consequences for the characterization of the flow behaviour will focus on methods using:

1. “flags”, applied by NREL in the early experiments
2. pressure flow probes.
3. stagnation pressure
4. several pressures at the airfoil surface e.g. at the nose. Matching with 2D pressures distributions as-well as calculated pressures are applied.

6.1 Flag technique

The flag technique comprises a vane on a probe in front of the rotor blade and gives directly the corresponding local flow angle. It was only applied by NREL during the experiments, phase II and III (Schepers et al, 1997),
In order to determine the upwash and dynamic characteristics of the flag, wind tunnel test were carried out with the flag sensor in front of the S809 airfoil. This configuration exactly resembles the outdoor experiment.
The equation for the upwash is plotted in figure 6.1 and is only related to the local flow angle at the flag which was established in the wind tunnel. This is a bit surprising because the cause of the upwash – the adjustment of the streamlines around the airfoil – is the lift generated by the airfoil. This implies that the upwash correction will not be accurate in case of augmented lift due to rotation, as is was not present during the wind tunnel experiments. Fig. 6.1 also show the different in upwash calculated with the well-known equation of Biot-Savart which is based on a single line vortex model approximating the airfoil. An earlier study [6.3] has shown that this could give very good results as long as the flags or probes are well in front of the lifting body. The differences between the values from the NREL equation and Biot-Savart are small for the attached flow but become considerable when stall occurs at -6. and 9. degrees. The investigation in the wind tunnel experiments of van Rooij (2002) did not indicate this deviation, however lo-

cal flow behaviour over the 2D model did deviate of the average span wise flow behaviour. Such difficulties and the fact that a closed wind tunnel section influences the flow lines as-well could have caused uncertainties in the derivation of the upwash correction. Applying the NREL data with the corrected inflow angle should therefore be considered with care.

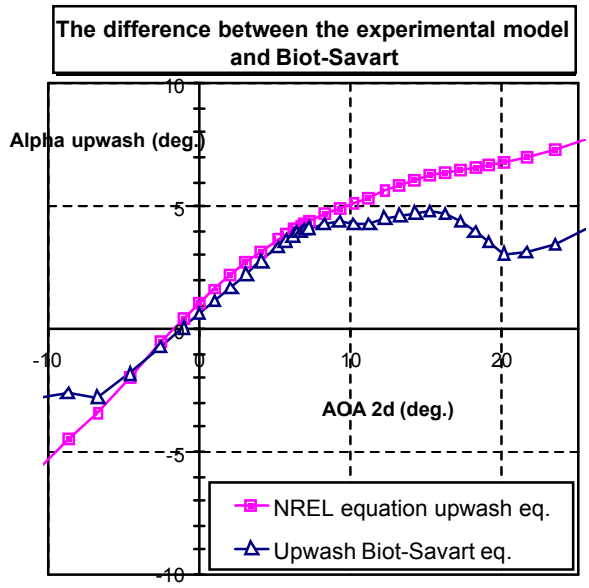

Fig. 6.1: The results from experimental derived equation of NREL compared with the simple Biot-Savart model.

The same upwash correction was used for the 5-hole flow probe at the NREL experiments as-well. This is an adequate solution because both flow devices were at (almost) the same position in front of the blade.

Apart from the distortion due to the upwash, the difference in span wise position of the flow devices and associated pressures results in an additional correction of the inflow angle in particular for a rotating blade. Such a correction – though small – was never included in the corrected angle-of-attack at the NREL experiments.

6.2 Flow probes

Flow probes of the multi hole pressure type were used in all field experiments. The derivation of the local flow angle is based on the difference in pressure between two opposite pressure holes in one plane. Including a stagnation pressure hole leaves a 3 hole probe as required minimum. Five, six or seven hole probe allows for derivation of the cross flow angle and the more holes available the more accurate the prediction of the flow angle will be. Unfortunately the increased number of calibration curves complicates the determination of the inflow seriously.
The configurations of the TU-Delft, NREL and Mie seem most promising because they had most of the probes close to the span locations with pressure taps. In particular the NREL configuration with 4 probes fitted 4% outwards the span locations with pressure taps was most suited. The initial probe positions on the TU-Delft rotor could unfortunately not be used and most of the measurements were carried out with only one flow probe at the 76% span location. This explains their search into techniques not based on flow probes.

The behaviour of the flow probes at the TU-Delft experiment (including a 3-hole and 5-hole) has thoroughly been investigated and the results can be found in (van Rooij, 2002). Here the data of the 3-hole probe is considered. The probe was positioned 0.55*chord in front of the blade. This is significant closer to the leading edge of the blade as for the NREL probes (0.81*chord).
The calibration curves for the probe include upwash and they were derived from wind tunnel experiments. The 3-hole probe is located 6% span outwards of the associated pressure orifices and a simple correction based on the oncoming wind speed was included.

Two measurement campaigns are selected to cover a fair part of the normal force coefficient curve and especially the performance just above 2D stall. To avoid uncertainties in inflow angle (due to e.g. damping in the pressure system) unsteady flow situations as well as tower shadow

interference and yaw are omitted from the time series. These selections has led to a reduction in data points of each campaign from 3100 to approximately 400 and are depicted in the left graph in Fig. 6.2. The spread in the derived angle-of-attack is large for normal force coefficients above 2D stall but limited below this value. Accuracy problems or flow phenomena could cause the large spread above stall.
Averaging of the several time intervals leads of course to a much smoother behaviour and the trends show a more gradual deviation towards higher inflow angles.

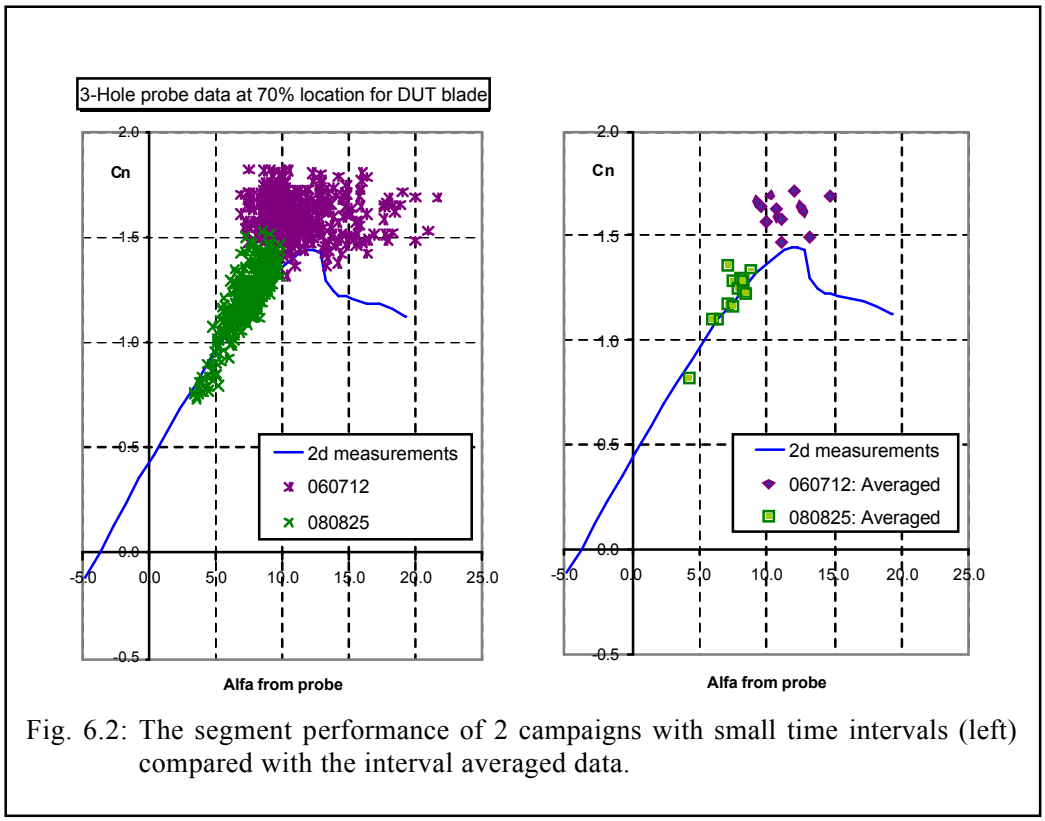

Fig. 6.2: The segment performance of 2 campaigns with small time intervals (left) compared with the interval averaged data.

The selection procedure leading to the average values was also used in the study on the NREL measurements with flag and flow probes and makes comparison between configurations much easier (van Rooij 2005)

6.3 Stagnation pressure

Most of the test set-ups with flow probes can determine the stagnation pressure (q_{stag}) from the probes or from the pressure distribution at the investigated span locations. The latter is preferred in particular to derive the pressure coefficient along the blade segment. This pressure can also be used to calculate the angle-of-attack from the velocity diagram with help of the rotational velocity. Figure 6.3 shows this angle in comparison with the angle-of-attack derived from the flow probes at the UAE experiment at the NASA wind tunnel. At this experiment the higher inflow angles were achieved and a more steady relation can be observed. The derived angle-of-attacks from the stagnation pressures are (almost) always larger than the values from the flow probe and its approximation improve towards higher tunnel speeds. This means that the acquired stagnation pressure is always larger then from calculations even including the tangential induction on the rotational speed. The local wind velocity had to exceed the tunnel speed. This trend was also observed in the measurements during the field experiment in Delft and it is not clear what is responsible for this behaviour because cross flow velocities are not regarded as sufficiently high.

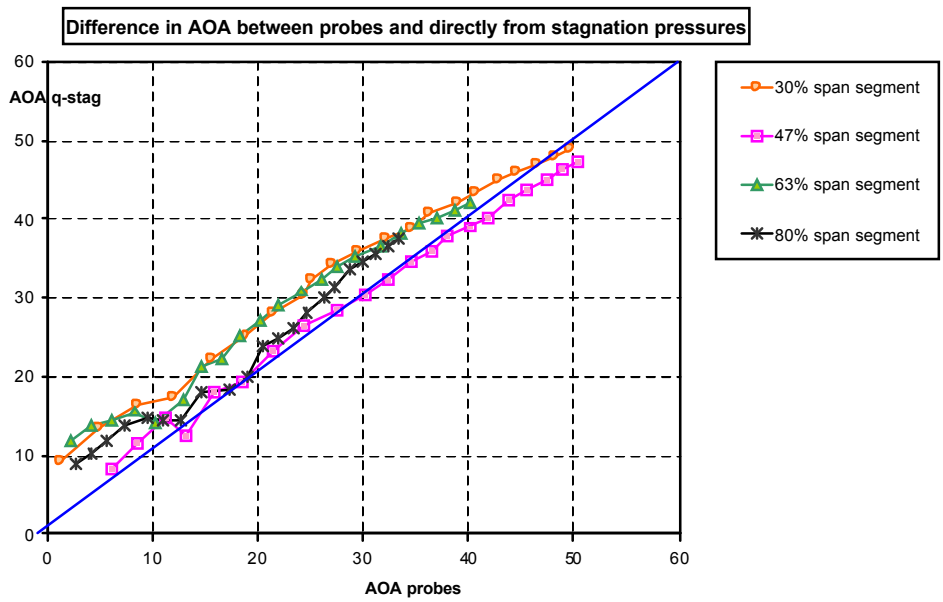

Fig. 6.3: The difference in derivation of the inflow angle in the steady flow configuration of the UAE experiment in the NASA Ames wind tunnel.

The deviation in stagnation pressure has always been a major issue in many discussions because it directly affects the non-dimensional pressure distribution Cp. For derivation of the inflow angle different methods were developed in which not the value but the location of the stagnation pressure was applied. Both ECN (Brand, 1994) and TU-Delft (Bruining, 1997) investigated this option and for the attached flow the results were sometimes quite satisfactory. In case of the TU-Delft method this was not surprising because it was based on the position of the stagnation point derived from wind tunnel measurements. The technique of ECN was different and not based on wind tunnel measurements, but did however not produce much better results. In particular not beyond 2D stall.

6.4 Nose pressures

6.4.1 From 2D measurements

The technique to derive the angle-of-attack from a number of pressures at the instrumented blade segment has been investigated by the TU-Delft. The background of the method lies in the fact that the head of a flow probe is rather similar to the nose of the airfoil and again two opposite pressures (or more) in one plane - here the upper and lower surface respectively - could be used to derive the inflow angle. Different orifice locations on upper and lower surface have been investigated and the upper positions at x/c_{up}= 0.007 and 0.073 and the lower surface at x/c_{lo}= 0.012 and 0.075 returned the best angle-of-attack. Calibration curves (orifice Cp with AOA) from the wind tunnel measurements with vortex generators at x/c=0.20 were applied to accommodate high normal force coefficients above 2D stall. A neural network method was used to determine the match between the obtained pressures and the four calibration curves. Depending on the conditions imposed on the neural network procedure like the so called spread, affect the number of solutions found. The sensitivity for this spread (accuracy interval) was small in case of the attached flow conditions but increased when the flow deviates from the 2D measurements.

The same measurement campaigns and selections as in case of the flow probe (par. 6.2) were used to show the segment performance at 70% span (Fig. 6.4). The graph includes the 2D performance with Vortex Generators and the derived segment performance matches very well due to similar pressure distribution near the nose. This indicates that characteristics with vortex gen-

erators on the NLF(1)-0416 airfoil are rather similar to the augmented lift on a rotating blade. Only 2.5% of the measured characteristics did not return a inflow angle.

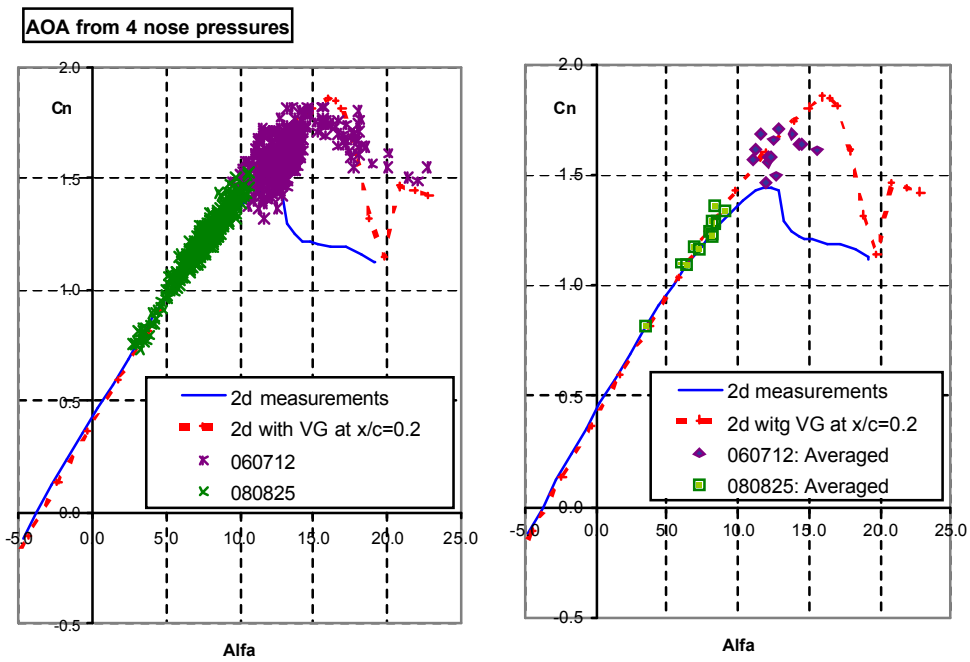

Fig: 6.4: The segment performance derived from the nose pressures for 2 campaigns with selected data and its averaged values.

The spread in angle-of-attack of the resulting normal force coefficient is much less then in case of the 3-hole flow probe (Fig. 6.2) especially above 2D stall. When the averaged values of the small time series are considered the difference between the flow probe and nose pressure technique is less pronounced which is due to the small the amount of data points.

Fig. 6.5 shows the difference between the two angle-of-attack derivation techniques. Again the largest scatter is found for the measurement campaign 060712 where even deviations up to 10 degrees occur which is very substantial in view of the approximated inflow angles close to 18 degrees. Most of the values differ less then 5 degrees in angle-of-attack and this is even less for the attached flow campaign 080825.

6.4.2 From RFOIL calculations

Instead of using 2D measurements as reference, it is possible to use 3D RFOIL calculations as a base. Lack of wind tunnel measurements are now no longer an obstacle and it opens the opportunity to include augmented lift due to rotation. In this investigation, rotational effects are included in the calculations using 2/3 of the geometric local solidity (c/r= 0.095). These pressure distributions are now used to derive the calibration curves required for the nose pressure technique. The calculated points and orifices should however be the same.
This approach has been used for the NLF(1)-0416 airfoil and the characteristics were similar to that of Fig. 6.4. The differences in derived angle-of-attack between the measurements and from the calculations can be observed in the right graph of Fig. 6.5. For the attached flow part the difference in angle is less then 0.5 degrees. Only for the few points beyond 20 degrees the differences exceed the 5 degrees. This means that application of the calibration curves from RFOIL show much better results than from the probe (Fig. 6.5, left graph). Of course this is only true under the assumption that the angle derived from the nose pressures of the 2D experiment (horizontal axis in graph 6.5) deliver the most reliable inflow angle.

In the investigation of (van Rooij 2003) other span locations at 30% and 50% and with different sets of (nose) pressure locations were evaluated. This resulted in segment characteristics beyond 2D stall. Changing the rotational parameter (c/r) in the calculations also showed that closer fits and increased number of realisations could be achieved. This could be an indication for the correctness of the with RFOIL calculated segment performance.

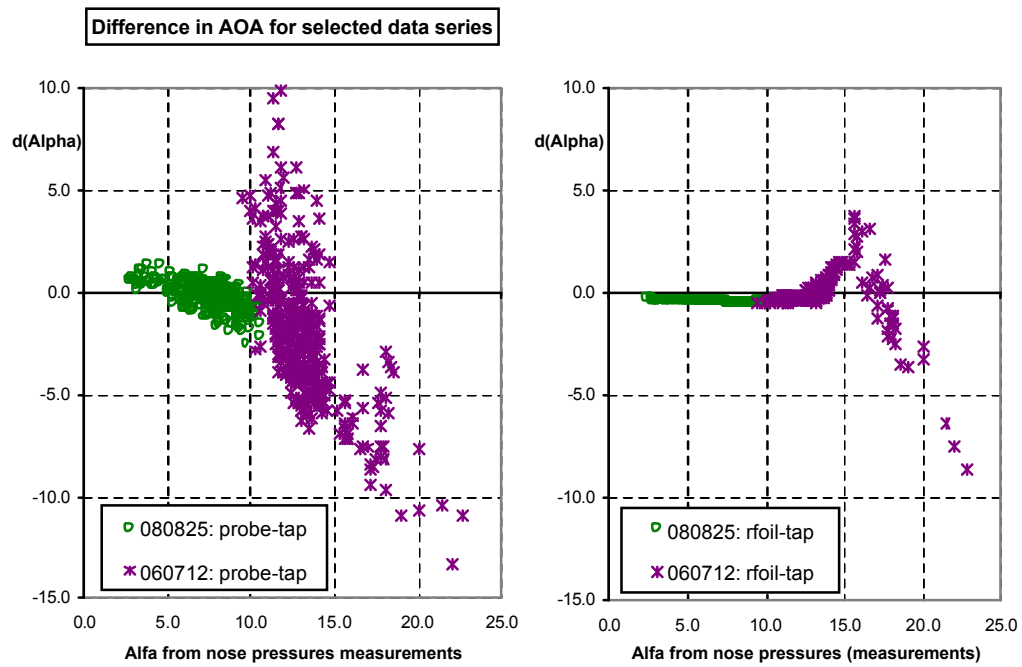

Fig. 6.5: The difference in angle-of-attack for the 3 methods of which the nose pressure technique is taken as reference.

6.5 Conclusions

From all investigated methods, the best results with the least scatter result from the nose pressures technique from wind tunnel measurements on the airfoil with vortex generators fixed at upper surface at x/c=0.2. This method does not need a correction for upwash nor a correction for the difference in span location like the flag or probe technique. However realisations for angle-of-attack can only be achieved when the pressure distributions at the nose resemble the input data. RFOIL could be helpful because with the rotational option of the program many different pressure distributions can be calculated close to the actual rotor data. This method fails in case of leading edge separation on a rotating blade. Switching to pressure data of solely the lower surface looks reasonably well.

7. Investigation of airfoil characteristics in IEA Annex XVIII database

In the Annexlyse project much effort was put on the analysis of the airfoil characteristics (i.e. the c_n-α and c_t-α characteristics) which are stored in the Annex XIV/XVII database (i.e. the c_n-α and c_t-α characteristics. From these characteristics the c_l-α and c_d-α characteristics can be derived if the angle of attack is known, see section 6. Observations on the characteristics are given in (Schepers 2003a; van Rooij 2003b; Schepers 2004a; Schepers 2004e).
A comparison between the measured characteristics and the characteristics obtained from different 3D models is given on the Annexlyse internet site:
http://www.ecn.nl/wind/other/annexlyse.html
The most important remarks on the comparison were the following:

- First it is noted that stall delay (i.e. the increase in c_l due to rotation at large angles of attack) is usually modelled by considering a factor f_{cl}. This factor is the ratio of the actual increase in c_l (i.e. c_{l3D}-$c_{l,2D}$) and the difference dc_l between the non-viscous $c_{l,potential}$ (with 'potential' slope $dc_l/d\alpha = 2\pi$) and the 2D value of $c_{l,2D}$. Hence

  $$f_{cl} = (c_{l,3D} - c_{l,2D})/(c_{l,potential} - c_{l,2D}) \quad (1)$$

  and

  $$c_{l,3D} = c_{l,2D} + f_{cl}(c_{l,potential} - c_{l,2D}) \quad (2)$$

  Other models (i.e. Corten, 2001; Lindenburg, 2003) relate the increase in $c_l(c_n)$ among others to the fraction of the chord which is stalled. This fraction is not measured in IEA Annex XVIII however by which such models are less straightforward to consider in the present project.

  In (Schepers, 2003) the measured rotating $c_l(c_n)$-α characteristics are compared with the corresponding 2D characteristics. It was found that f_{cl} should be a function of c/r, pitch angle, rotor speed and the angle of attack. A number of 3D stall models were considered but none of them took all of these dependancies into account .

- In the 3D stall model from the University of Illinois (Du, 1998) the rotor speed dependency of f_{cl} is modelled. Thereto, f_{cl} is assumed to depend on a modified tip speed ratio:
  $\Lambda = \Omega . R / \sqrt{((\Omega . R)^2 + U_{hub}^2)}$
  For all measurements which are considered in the present project, this tip speed ratio is between 0.97 and 1.0. The sensitivity of the factor f_{cl} to these variations in Λ is, at least according the model of (Du, 1998) negligible. For this reason the rotor speed dependency is neglected in the sequel;
- In figure 7.1, a representative example of $f_{meas}(\alpha)$ is given where f_{meas} is the value of f_{cl} derived from the measured $c_l(\alpha)$ curve of the NREL phase IV experiment at 30% span. The measured values are compared with model results:
  f_{ECN} denotes the value from Snel (1993). The model is based on the following expression:

  $$f_{ECN} = 3.(c/r)^2 \quad (3)$$

  f_{CRES} denotes the value from a model developed by CRES (Chaviaropoulos, 2003).
  This model is based on the following expression:

  $$f_{CRES} = 2.2(c/r)\cos^4(\epsilon + \theta_p) \quad (4)$$

Figure 7.1 shows that initially, f_{meas} increases with α. A maximum is reached near $\alpha \sim 20$ degrees.
Thereafter the factor f_{cl} decreases again. The models from CRES nor ECN include such dependency on the angle of attack. It may, however, implicitly be included in the models from (Lindenburg, 2003) and (Corten 2001)

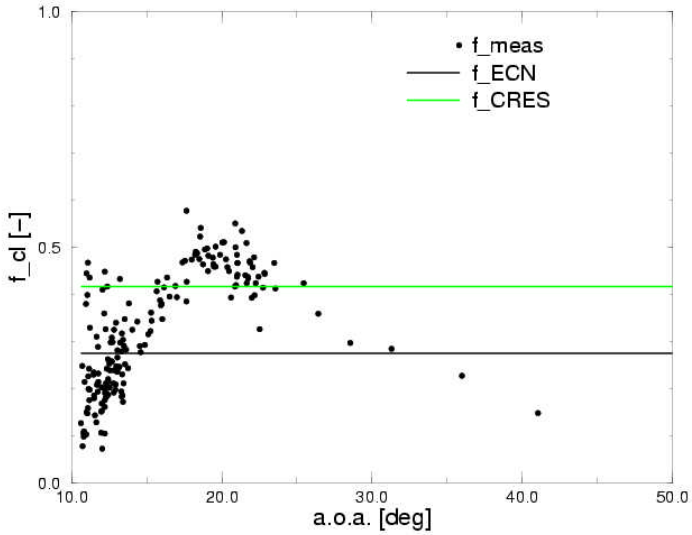

Figure 7.1: *Factor f_{cl} as function of* a *for the NREL Phase IV experiment at 30% span*

Furthermore, figure 7.1 shows f_{ECN} to be too low, where f_{CRES} is more realistic (at least near an angle of attack of 20 degrees). This observation turned out to be valid for the measurements of the other IEA Annex XVIIII facilities as well.

- In figure 7.2 the values of f_{cl} are presented as function of c/r. Some explanatory comments should be given to this figure: The factor f_{cl} is determined from a large number of $c_l(\alpha)$ measurements: To this end, the measurements on all instrumented sections on the two NREL rotors, the RISØ rotor and the DUT rotor are considered. Some slight adjustments have been made to the measured angle of attack in order to fit the 3D c_l-α curve to the 2D curve. This results in a large number of figures, similar to figure 7.1. Then the factor f_{cl} at $\alpha \sim 20$ degrees is approximated visually and these values are plotted as function of c/r in figure 7.2. As a matter of fact, the results from DUT and NREL Phase II are most suitable to derive the c/r dependency, since these turbines have untwisted blades. For all other turbines a different c/r is by definition associated with a different twist, which is expected to influence the factor f_{cl} as well, see equation 4. Therefore the values of f_{cl} for the RISØ and NREL Phase IV turbine, have been corrected for the twist under the assumption that f_{cl} varies according to $\cos^4(\varepsilon+\theta_p)$ consistent with the assumption from equation 4. The measurements from DUT yield the following c/r dependency:

$$f_{cl} = 1.5558\left(\frac{c}{r}\right)^{0.5645} \qquad (5)$$

The NREL Phase II measurements yield:

$$f_{cl} = 4.9287\left(\frac{c}{r}\right)^{1.5369} \qquad (6)$$

The best fit on all measurement points (including the NREL Phase IV and RISØ measurements with a pitch angle correction) is found to be:

$$f_{cl} = 2.93(\frac{c}{r})^{1.178} \qquad (7)$$

Expression 7 is very close to relation 4 for zero pitch angle:
$f_{CRES} = 2.2 \cdot (c/r)$

Recently there has been some discussion on the proper c/r dependency. The linear c/r is associated to the so-called centrifugal pumping mechanism, see (Corten, 2001; Lindenburg, 2003) where equation 3 assumes a quadratic $(c/r)^2$ dependency. The present results indicate that, in general, a linear dependency is closer to the measurement data.
The large differences between the expressions 5, 6 and 7 throw some doubt on the assumption that a generally valid expression for the c/r dependency exists. It should be realised however, that the expressions are determined in a rather crude way due to the uncertainties in the angle of attack, the basic 2D characteristics, the visual averageing etc.;

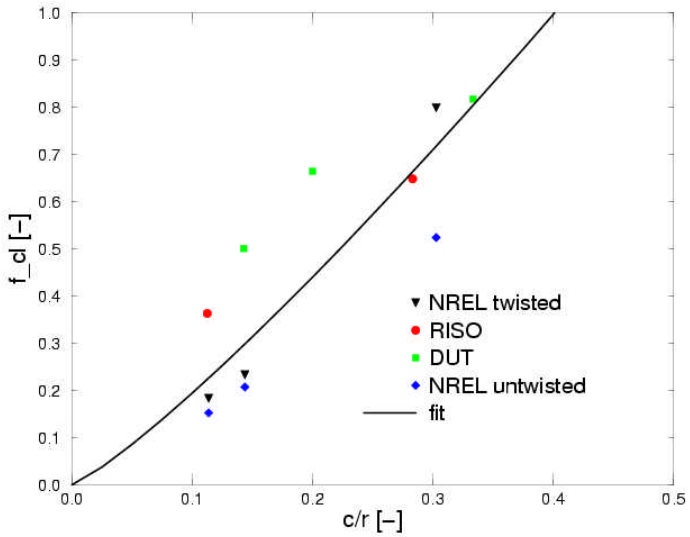

Figure 7.2: *Factor f_{cl} as function of c/r from the available IEA Annex XVIII measurements*

- In (Schepers, 2003a) measurements are presented from ECN and NREL, which show a clear dependency of the c_n-α curve on the pitch angle (θ_p): Stall delay effects appear much stronger at negative pitch angles, which due to the positive twist (ε) implies a small total blade angle: $\varepsilon + \theta_p$. The only known 3D model which does account for such dependency is the model from (Chaviaropoulos, 2003). This model assumes a $\cos^4(\varepsilon+\theta_p)$ dependency for f_{CRES}, see equation 4. In figure 7.3 the measured values of f_{cl} (at $\alpha \sim 20$ degrees) are shown as function of $\varepsilon+\theta_p$ for three instrumented sections of the NREL Phase IV rotor. The factor f_{cl} is normalised to its maximum value at every instrumented section which, in agreement with equation 4 is found at $\varepsilon+\theta_p$ closest to zero indeed. As such the model from CRES reproduces the behaviour from figure 7.3 very well in a qualitative way. Nevertheless the measurements from figure 7.3 show a stronger drop in f with increasing values of $\varepsilon+\theta_p$ than the $\cos^4(\varepsilon+\theta_p)$ dependency from f_{CRES};

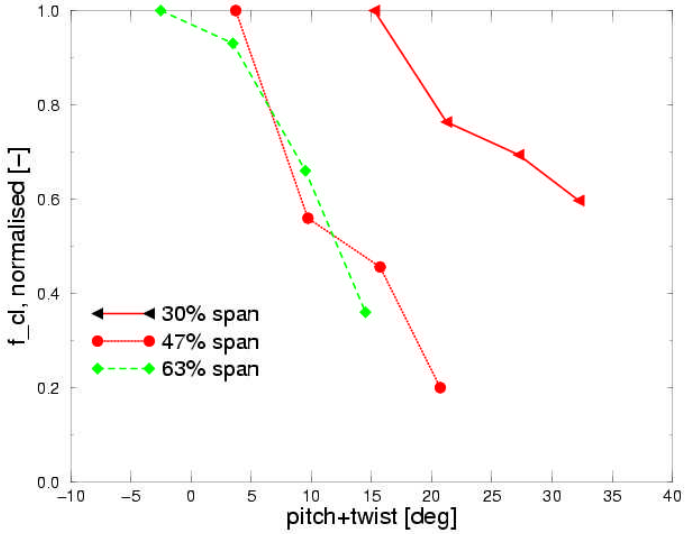

Figure 7.3: *Normalised factor f_{cl} as function of pitch angle (+twist) for the NREL, Phase IV measurements*

- In (Schepers, 2003a) it is shown that most c_t-α curves are over predicted. This led to the suspicion that the drag coefficients are under predicted. The model from CRES, as described above, does forecast an increase in drag coefficient by applying the factor f_{CRES} from equation 4 to the difference between the 2D drag coefficient and the minimum drag coefficient. Hence:

$$c_{d,3D} = c_{d,2D} + f_{cd}.(c_{d,2D} - c_{d,2D,\min}) \qquad (8)$$

  with f_{cd} from equation 4. The increase in lift due to rotation is associated to the increased suction pressures. Since viscous drag is negligible at higher angles of attack, the increased drag should also be apparent in the pressure distribution, but this is less transparant than it is for the lift. This is due to the fact that the drag forces are related to the pressure differences between the 'front' and 'rear' part of the airfoil. As such increased suction pressures at the rear part of the airfoil increase the drag, but this is opposed by increased suction pressures at the leading edge. Now, from a physical point of view it can be doubted whether the f-factor in the drag modelling should be similar to the f-factor in the lift modelling, as is the case in the model from (Chaviaropoulos, 2003). This would imply that the modified pressure distribution effects the resulting force in normal direction similar as the force in tangential direction, which is difficult to believe. Although measurements of c_d have been supplied to the IEA Annex XVIII database, they are not expected to be a reliable basis for an engineering relation of the drag (if such relation exists at all). This is a result of the uncertainty in the tangential force (section 5) which, multiplied with the very uncertain $\sin(\alpha)$ term, forms an important contribution to the drag force. Nevertheless the NREL c_d measurements have been analysed in a qualitative way (see the comparison on http://www.ecn.nl/wind/other/annexlyse.html): They show f_{cd} to depend on α where the maximum in f_{cd} seems to appear near $\alpha \sim 15$ degrees and is much (> 6 times) higher than the factor f_{CRES} from equation 4.
- In (Schepers, 2003a) it is shown that near the tip section (r/R > 9) both the c_n-α and the c_t-α curves are considerably over predicted.

8. Comparison between calculations from aero-elastic code PHATAS and IEA Annex XIV/XVIII measurements

In the previous section various 3D models were related to measurements of aerodynamic characteristics as function of angle of attack. It is known however (see sections 4 and 6) that the measured aerodynamic characteristics suffer from large uncertainties.
This is mainly caused by the uncertainty in angle of attack and dynamic pressure which both effects the segment coefficients.
To avoid these uncertainties, the aerodynamic data from the IEA Annex XVIII database have also been applied in a different way:
ECN's aero-elastic code PHATAS, see (Lindenburg, 1999) is used to simulate time series from the IEA Annex database. Measurements from DUT, ECN, NREL (both the twisted as well as the untwisted blade) and RISØ, at more or less aligned conditions have been simulated.
Then the calculated and measured, time averaged, dimensional, aerodynamic segment loads are compared. Moreover, the comparison on aerodynamic segment loads is related to the comparison on the overall blade and rotor loads (flatwise moments, rotorshaft torque and axial force), which are quantities which are of direct importance for designers. The main advantage of such comparison lies in the fact that the dimensional forces are not obscured by the uncertainties in dynamic pressure nor angle of attack, which do effect the comparison on dimensionless characteristics, and which are known to yield substantial uncertainties. Furthermore the local aerodynamic effects are directly related to design loads. As such, the comparison is believed to give a good insight into the most important sources of discrepancies and it can form the basis for suggestions for model improvement. The results of this investigation can be found in (Schepers, 2004a; Schepers, 2004e).

The calculations have been performed using the standard PHATAS-IV version, see (Lindenburg, 1999).
The geometrical and structural PHATAS input is based on the descriptions of the IEA Annex XVIII report, see (Schepers, 2002). A comparison with measured overall data (masses, eigenfrequencies centre of gravities etc.) showed a good agreement. The 2D airfoil characteristics which have been used in the PHATAS calculations, are based on characteristics from the Aerodynamic Table Generator (ATG, see Bot, 2001).The ATG is a database with measurements of 2D airfoil characteristics with inter(extra) extrapolations to generate performances for a wide range of angles of attack, thicknesses and Reynolds numbers.
The 2D c_l-α curves have been corrected for 3D effects according to the model of (Snel, 1993), which was already described in section 7.
In the PHATAS calculations, the wind speed was assumed to be constant (with wind shear included).

The present report will only show a fraction of the comparisons made. The interested reader is referred to the Annexlyse Internet site:
http://www.ecn.nl/wind/other/annexlyse.html. On this site the full comparison can be found and additional analyses are given for the IEA Annex XVIII measurement data.

The present paper highlights some results and the comparison with measurements on the NREL rotor with twisted blades (Phase IV) will be discussed in more detail. These results are usually very representative to the results which are obtained on the DUT rotor, the ECN rotor, the untwisted NREL rotor and the RISØ rotor.
For the Phase IV turbine, 5 campaigns are analysed at (more or less) aligned flow conditions. They are denoted as campaign 1 to 5, see table 1. Note that α_5 denotes the mean measured angle of attack at 95% span and the mean rotorspeed is 72 rpm.
The main difference is in the wind speed. The wind speed is lowest for campaign 1 and highest for campaign 5.

The measurement period is 1 minute. Although this is a relatively short period, the present study mainly considers mean values for which the measurement period is less important (although certainly not fully unimportant) compared to studies on dynamic effects.

Campaign	α_5 (deg)	U_{hub} (m/s)	Power (kW)	θ_p (deg)
1	4.3	7.1	3.3	3.0
2	9.4	10.4	9.7	3.0
3	12.1	12.9	11.1	2.6
4	15.2	15.9	9.4	2.7
5	18.4	19.3	10.1	2.9

Table 3: *Global conditions of NREL measurement files*

The sections where the aerodynamic forces are measured (relative to the rotor centre) are located at 30%, 47%, 63%, 80% and 95% span.
In the figures 8.1 and 8.2 the ratios between calculated and measured normal forces and tangential forces (i.e. the calculated value divided by the measured value) are presented as function of mean wind speed. In figure 8.3 the ratios between calculated and measured root flatwise moments and rotorshaft torques are given.

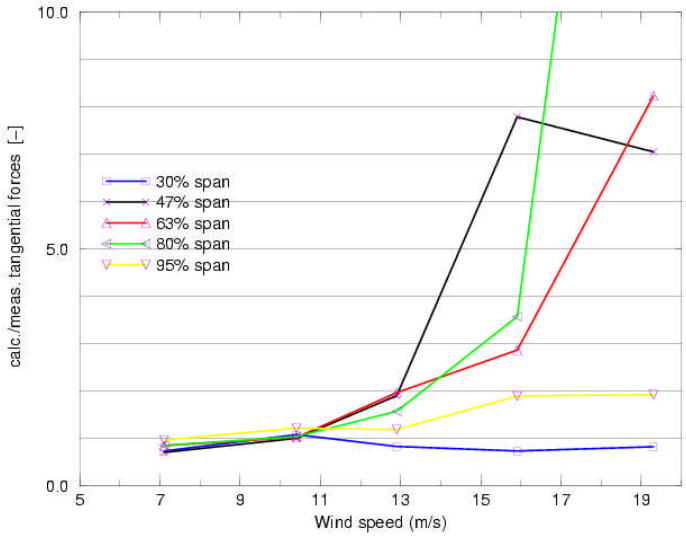

Figure 8.1: *Ratio between calculated and measured tangential forces of NREL Phase IV campaigns(time averaged)*

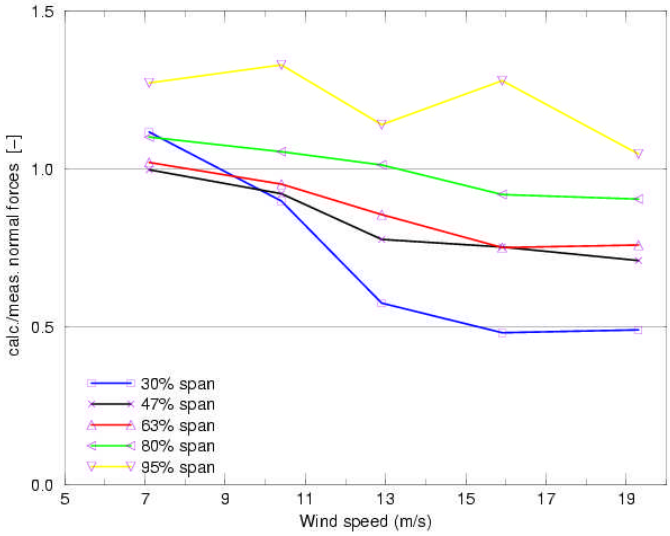

Figure 8.2: *Ratio between calculated and measured normal forces of NREL phase IV campaigns (Time averaged)*

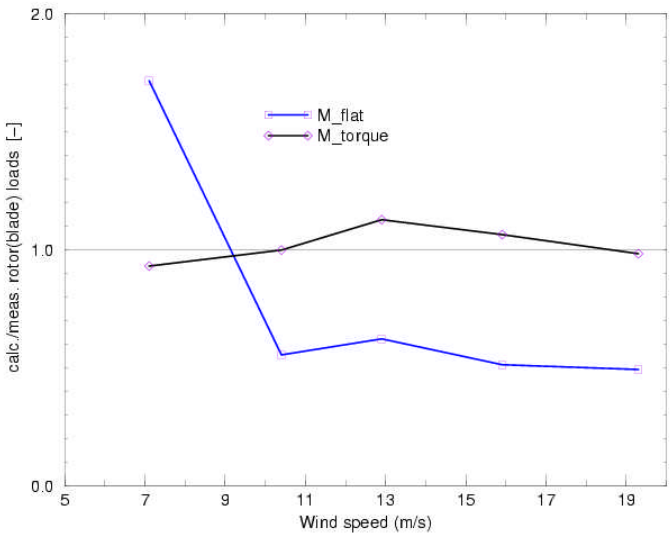

Figure 8.3: *Ratio between calculated and measured flatwise moments and torque of NREL phase IV campaigns (Time averaged)*

The ratios, which are presented in the figures hide the sign information of the underlying loads. The normal force and flatwise moment were usually directed in 'downwind' direction, where the tangential force is pointing towards the leading edge.
The following comments can be made to the comparison (where it is emphasized that the comments for the DUT, ECN, NREL untwisted rotor and the RISØ rotor are largely similar):

- Tangential forces, see figure 8.1 The relative differences in tangential forces are generally large. Usually the value of the tangential force is over predicted, i.e. the ratio is (far) above

1, although this is less true for the inner station for the present NREL measurements (For most other turbines this is also true at the inner station). Note that this observation is consistent with the observation on the c_t-α characteristic from section 7. This implies the prediction of a too strong force towards the leading edge (i.e. a more negative tangential force). The stronger force towards the leading edge can be a result of an over predicted lift force but it can also be a result of an under predicted drag force. The latter is in principle always true due to the neglect of the skin friction but this contribution is only significant at small angles of attack.

- Normal forces, see figure 8.2: A large under prediction of n_1 (30% span) is found at the high wind speeds (the cases 4 and 5). The value of n_4 (80% span) is over predicted at the low wind speeds, but at the high wind speeds this force is under predicted. The value of n_5 at the very outer station (95% span), is always over predicted. This is consistent with the over predicted normal force characteristic which was already mention in section 7. The tip effects are modelled according to the well known Prandtl tip correction, which only corrects for the finite number of blades. An explicit tip loss, due to the finite length of the blade is not taken into account.
- Correlation between local aerodynamic loads and overall rotor loads, see figure 8.3: The differences between calculated and measured torque are very small. This is a surprising result, in view of the large discrepancies between the normal forces and tangential forces. Note that at least the measurements of the normal force and the torque are believed to be reliable, see section 5. Then the good agreement in torque seems to be due to compensating 'errors' between normal and tangential forces: The normal force is generally under predicted (yielding a lower torque) and the tangential force is over predicted (yielding a higher torque). Hence a good agreement in rotor loads is found even if the associated segment forces are predicted very poorly. It is again emphasised that similar observations are found for the other turbines in IEA Annex XVIII, where, additionally, it was found that 'errors' between loads on the inner part of the blade could be compensated by 'errors' on the outer part of the blade. The largest under prediction of the flatwise moments is found for campaign 4 and 5, which also show the largest under prediction of the normal forces.

9. Recommendations on model improvement for aero-elastic load calculations

9.1 Suggested model improvements

The considerations from the sections 7 and 8 have led to the following recommendations:

- A model should be developed which, compared to the original PHATAS modelling, yields higher normal forces at the root sections. Furthermore the tangential forces (i.e. the force towards the leading edge) should be decreased for all sections. For the tip sections (r/R > 0.9) both the normal as well as the tangential force should be decreased. Finally the dependency of f_{cl} on the pitch angle and angle of attack should be taken into account where the dependency on c/r should be as close as possible to the behaviour found in equation 7.
- The model from (Chaviaropoulos, 2003) could form the basis for most of these improvements. This model had already included the pitch angle dependency and a c/r dependency which is close to equation 7. The relative high values for f_{cl} which result from the CRES model are expected to yield higher values of the normal force, closer to the measured data. Moreover the increased drag from the CRES model will reduce the tangential forces in agreement with the measured results.

Hence the model from CRES has been used as starting point, but some further refinements by means of 'trial and error' were applied.
Thereto several parameters were varied systemetically until the resulting local aerodynamic loads as calculated by PHATAS, showed an acceptable agreement with most measured loads.

- Lift modelling (i.e. f_{cl})

  - Pitch angle and c/r dependency:
    The $\cos^4(\varepsilon + \theta_p)$ dependency is enhanced to a $\cos^6(\varepsilon + \theta_p)$ dependency, since the measurements from figure 7.3 indicate a stronger $(\varepsilon + \theta_p)$ dependency. The c/r dependency was enhanced to a $(c/r)^{1.4}$ dependency;
  - Angle of attack dependency:
    It was attempted to reproduce the behaviour from figure 7.1. The maximum value of f_{cl} was assumed to appear at α=20 degrees.

$$f_{cl,a=20} = 3.8(c/r)^{1.4}\cos^6(e + q_p) \qquad (9)$$

    The angle of attack dependency has then been modelled in the following way:
    An initial increase in f_{cl} until $\alpha = 20$ degrees is modelled. This increase is assumed to be proportional to dc_l i.e. $c_{l,potential} - c_{l,2D}$. This difference increases with angle of attack. $f_{cl} = (dc_l / (dc_l(\alpha=20)))^* f_{cl}(\alpha=20)$ by which, see equation 1, the actual value of $c_{l,3D}$ becomes proportional to dc_l^2. Between 20 and 25 degrees the factor f_{cl} remains constant. Between 25 and 60 degrees, the factor f_{cl} drops linearly to zero.

- Drag modelling (i.e. f_{cd}) :
  The drag model is written in the form of equation 8. Because, as mentioned above, the direct IEA Annex XVIII measurements on c_d were believed to be rather inaccurate most dependancies in the drag model were just copied from the lift model, where information on the angle of attack dependency from the NREL c_d measurements was only used in an indicative way. Then multiplication factors have been determined by means of trial and error. In summary this gave the following model:

- Pitch angle and c/r dependency:
  The dependency on the pitch angle and c/r remained similar to the dependency from equation 9, i.e. a $(c/r)^{1.4}$ dependency and a $\cos^6(\varepsilon + \theta_p)$ dependency;
- Angle of attack dependency:
  The factor f_{cd} is assumed to be maximum at $\alpha = 15$ degrees. This maximum is defined to be:

$$f_{cd,a=20} = 6.0 * 3.8(c/r)^{1.4} \cos^6(e + q_p) \qquad (10)$$

  Hence the maximum value of f_{cd} is 6 times the value of the maximum f_{cl}. The value of f_{cd} increases until $f_{cd,\alpha=15}$ by making it proportional to the value of d_{cd}, i.e. $(c_{d,2D} - c_{d,2D,min})$. Between α is 15 degrees and α is 20 degrees the value of f drops linearly to

$$f_{cd,a=20} = 2.5 * 3.8(c/r)^{1.4} \cos^6(e + q_p) \qquad (11)$$

  Between $\alpha = 20$ degrees and $\alpha = 30$ degrees, f_{cd} remains constant to the value from equation 11 and between $\alpha = 30$ degrees and $\alpha = 45$ degrees, f_{cd} drops linearly to zero.

- Tip modelling. The tip modelling has been modified, using a tip loss model developed by DTU, see (Shen, 2003). This model is based on wind tunnel measurements made by NREL and FFA, on 2-bladed turbines. It explicitly reduces the lift force coefficient and the resultant normal forces and tangential force coefficients to zero at the tip. The tip correction modelling differs (only for 3 bladed rotors) from the one described in (Shen, 2003), since the original model did not give a satisfactory results for 3-bladed rotors.

9.2 Model modifications: Comparison between aeroelastic code calculations and IEA ANNEX XVIII measurement data

The calculations, which have been presented in section 8 have been repeated using the model modifications described in section 9.1. In the figures 9.1, 9.2 and 9.3 the ratios between calculated and measured normal forces, tangential forces, flatwise moments and rotor shaft torques are presented in a similar way as in section 8. It is recalled that the conditions of the different campaigns can be found in table 1.

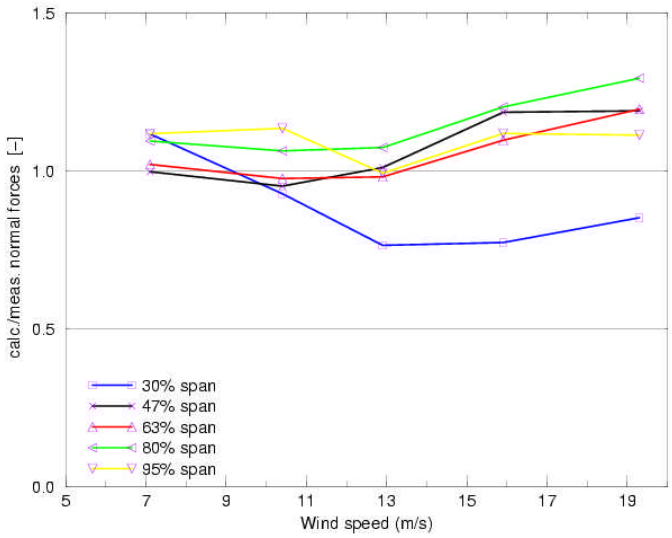

Figure 9.1: *Modified modelling: Ratio between calculated and measured values of the normal forces for the NREL phase IV campaigns (time averaged)*

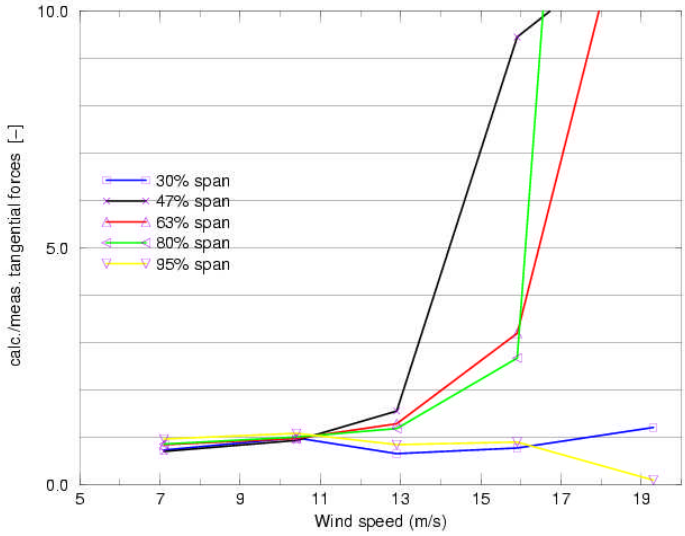

Figure 9.2: *Modified modelling: Ratio between calculated and measured values of the tangential forces for the NREL phase IV campaigns (time averaged)*

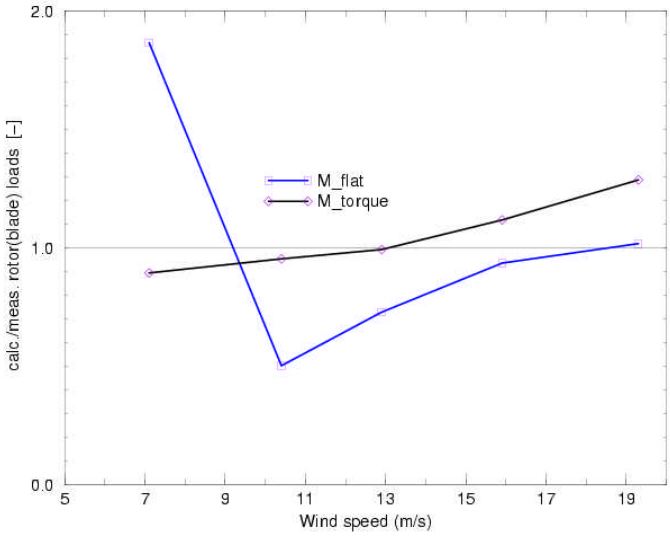

Figure 9.3: *Modified modelling: Ratio between calculated and measured values of the flatwise moment and the rotorshaft torque for the NREL phase IV campaigns (time averaged)*

The following observations can be made:

- The normal forces at 30%, 47% and 63% span are predicted much more accurately in particular at the high wind speed cases 4 and 5 (compare figure 8.2 with figure 9.1). The better prediction of the normal forces is reflected into a more accurate prediction of the flatwise moments, compare figure 8.3 with figure 9.3;
- The normal forces at the very tip (the 95% section) are predicted much more accurately;
- The tangential forces are still over predicted (compare figure 8.1 with figure 9.2). This is a result of the higher values of the lift, which are only partly compensated by the higher drag

from equation 11. As a consequence, the rotor shaft torque is slightly over predicted. It should be noted however, that the good agreement in torque from the original modelling is very misleading, since it is the result of two compensating errors: An under predicted normal force in conjunction with an over predicted tangential force. It might be tempting to increase the drag from equation 11. This did improve the agreement with the NREL measurements indeed, but the agreement with the measurements on the other facilities became poorer. Hence the present model should be considered as a 'common denominator' of all IEA Annex XVIII facilities.

10. Yawed conditions: Measurements and modelling

Modelling of yawed conditions is known to be one of the major deficiencies in current wind turbine design codes. In the past, large discrepancies have been found in the prediction of mechanical loads at yawed conditions and in particular the prediction of yawing moments (and stability) suffered from large uncertainties, see (Snel, 1994; Schepers, 1995).
In task 3.4 of the Annexlyse project, the IEA Annex XVIII measurements at yawed conditions are analysed. Among others, a comparison is made with the results from PHATAS-IV. The results are reported in (Schepers, 2004d).

The main emphasis in the investigation was on the prediction of the yawing stability (or more specific: the variation of wind turbine loads over the rotor plane). This stability is partly determined by the variation of the induced velocity over the rotor plane, caused by the skewed wake geometry. The variation in induced velocities yields a load unbalance between the upwind and downwind side of the rotor plane and as such a yawing moment.

Until 1990, wind turbine design codes did not predict this load unbalance and resulting yawing moments at all. Yawed conditions were only modelled through the so-called advancing and retreating blade effect, which basically adds or substracts the tangential free wind speed component to the rotational speed. The effect is explained in figure 10.1 (left).
In this figure the definition of the positive yaw angle and the definition of the azimuth angle (zero when the blade points down at 6 o'clock) is also given.
For positive yaw, the blade will be retreating in the upper half plane and advancing in the lower half plane with respect to the in plane wind component V_{tang} This gives a 1P variation of angle of attack and effective inflow velocity: The advancing and retreating blade effect results in a symmetric load distribution along the vertical line in the rotor plane. Such load distribution yields a neutral yawing moment, where it was known from measurements that the real yawing moment is stabilizing (i.e. restoring).

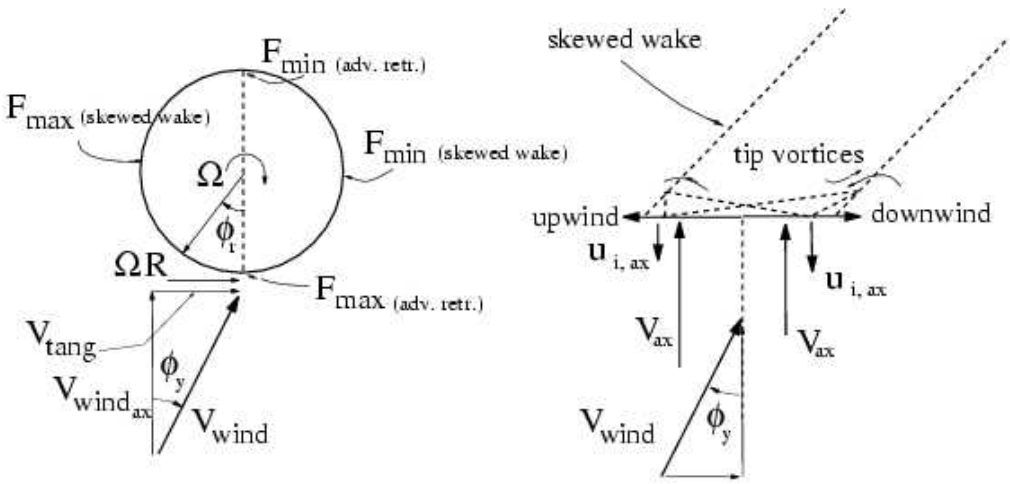

Figure 10.1: *Advancing and retreating blade effect; definition of azimuth and yaw angle*

This was one of the reasons to perform the EU Joule projects on Dynamic Inflow (see Snel, 1994; Schepers, 1995) in the period 1990-1995. The models developed in these projects did not only include the advancing and retreating blade effect, but also the effect of the skewed wake geometry on the inflow distribution, see figure 10.1 (right):
The proximity to the rotor plane of the vortices in the wake strongly influences the inflow. The trailing tip vorticity is on the average closer to the downwind side of the rotor plane, which according to the Biot-Savart law results in a larger value of the axial induction velocity $u_{i,ax}$
The higher induced velocity means a lower value of the total axial velocity for the downwind half of the rotor plane and hence lower blade loads in this part. The resulting load unbalance yields a restoring yaw moment.
The models developed in the Dynamic Inflow projects, basically originate from helicopter theory and assume a sinusoidal variation of the inflow velocity with the maximum velocity at the upwind side of the rotor plane. Such inflow distribution generally led to a stabilizing yawing moment indeed, which was already a considerable improvement compared to the previously used 'advancing and retreating models'.

However, the results of a Dutch national project, performed in 1998, showed these sinusoidal models to be deficient as well. In that project, see (Schepers, 1999), a model rotor was placed in the open jet wind tunnel of the University of Delft and direct measurements of the inflow distribution in its rotor plane were made. The measurements have been used to improve the yaw model in the PHATAS code. It was found that the real inflow distribution differs considerably from the expected sinusoidal distribution. This was in particular true near the root of a blade where the root vorticity even makes the maximum velocity to occur at the downwind side of the rotor plane. This then tends to destabilize the yawing moment. This is illustrated in

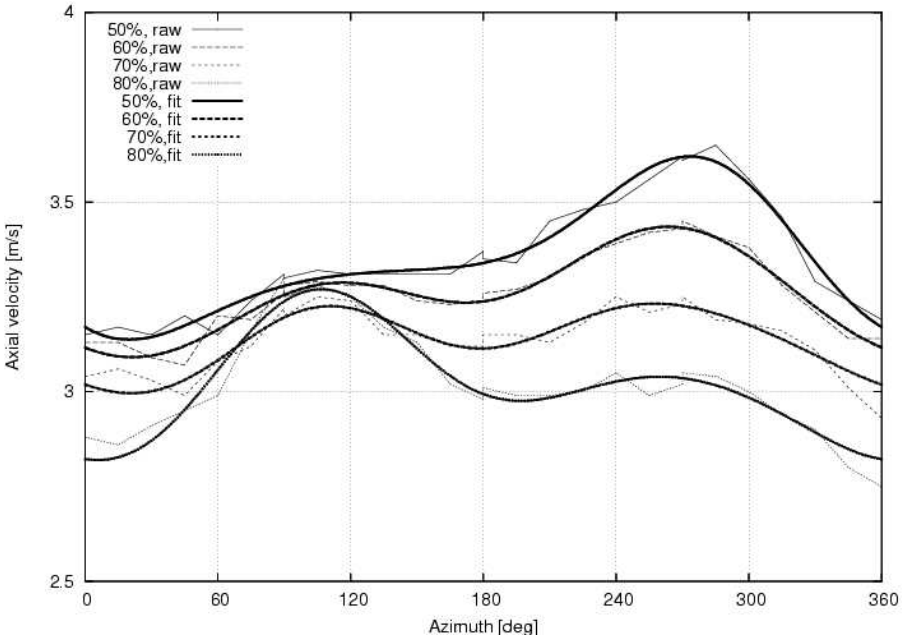

Figure 10.2: *Measured axial velocity at 30 degrees yaw in DUT open jet tunnel*

figure 10.2 which shows a representative measurement result of the axial velocity V_{ax} (i.e. $V_{wind} - u_{iax}$) at a positive yaw angle of 30 degrees. The raw measurements are presented, together with a third order Fourier fit. Despite the scatter in the raw measurement results, a clear trend is visible. This trend appeared not only at 30 degrees yaw but also at 45 and 60 degrees. Most important is that at the inner part of the blade, the maximum value of V_{ax} is reached at $\phi_r = 270$ degrees. This implies that the maximum axial velocity is at the downwind part of the rotorplane (between 180 and 360 degrees azimuth at positive yaw, see figure 10.1)
Probably the same holds for the loads by which the inner part of the rotor is expected to contribute to a destabilizing yawing moment!

At the outer part of the blade, the absolute maximum shifts to $\phi_r = 90$ degrees resulting in a stabilizing yawing moment.
As a consequence the inflow distribution at the tip becomes more similar to the expected sinusoidal distribution. Nevertheless at $\phi_r = 270$ degrees a local maximum is still apparent. This makes the yawing moment less stabilizing than the yawing moment which results from a sinusoidal inflow distribution.

The deviation from the expected sinusoidal behaviour could be explained by root vorticity effects which were not considered in the development of the sinusoidal velocity models. Obviously the inflow measurements from (Schepers, 1999) only gave indirect information on the load distribution. Non-linear aerodynamic effects, but also the advancing and retreating blade effect as well as flexibilities, wind shear, tilt angle, etc make the relation between the inflow variation and the load variation less straightforward. Therefore a direct validation of the load variation at yawed conditions is extremely useful. The IEA Annex XVIII measurements offer the material for such validation. The main aim of the present analysis has therefore been to investigate whether the root can contribute to a destabilizing yawing moment where at the same time the tip can contribute to a stabilizing yawing moment.

10.1 Results

A number of IEA Annex XVIII measurements have been selected for further analysis. The campaigns should fullfill the following criteria:

- The campaign should be taken at a substantial (mean) yaw angle (> 15 degrees);
- The averaged axial induction factor (which obviously only can be derived from calculations) should be > 0.15. At lower axial induction factors the loading variation over the rotor plane is mainly determined by the advancing and retreating blade effect;
- The wind shear should be measured. This is an important requirement because the loading variation over the rotor plane interferes with the variation which is caused by wind shear and their effects are difficult to distinguish;
- Preferably the yawed campaign should be compared with a similar campaign at (almost) zero yaw.

Then the only campaigns, which satisfy these criteria have been measured on the ECN facility.

The aerodynamic normal forces at different radial stations of the selected campaigns are binned on azimuth angle and compared with the results from PHATAS-IV.
A representative results at 30% span for a positive yaw angle of 43 degrees is shown in figure 10.3. The result for 80% span is shown in figure 10.4. Results for (more or less) zero yaw are also added.

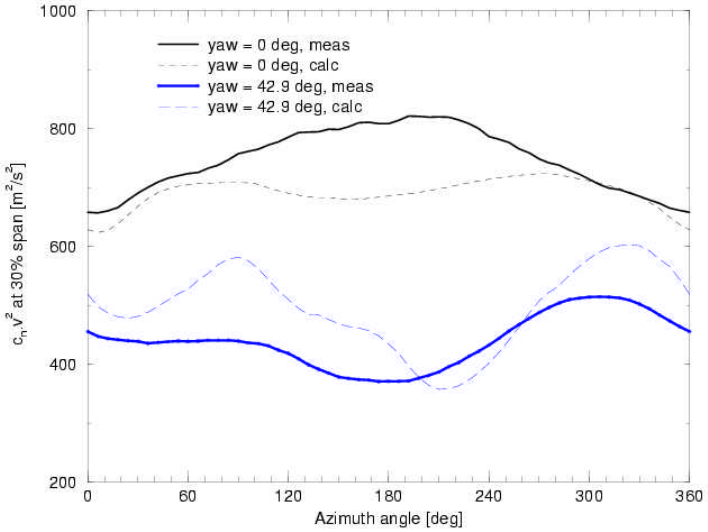

Figure 10.3: *ECN campaign: n-f_r at f_y = 42.9 deg and at a » 0.2; 30% span*

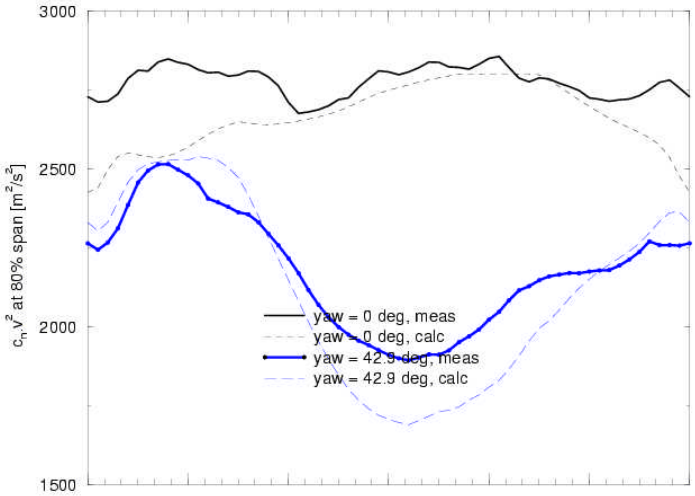

Figure 10.4: *ECN campaign: n-f_r at f_y = 42.9 deg and at a » 0.2; 80% span*

The measurements show that at the root (i.e. at 30% span) the maximum force is found at the downwind side of the rotor plane (near $\phi_r \approx 310$ degrees) corresponding to a destabilizing yawing moment. At the tip (i.e. at 80% span) the maximum is found at the upwind side of the rotor plane (near $\phi_r \approx 50$ degrees).
Generally speaking the PHATAS-IV results show a good agreement with the measured results. Most important is that they also predict the destabilizing yawing moment contribution at the root where at the same time, the tip is predicted to contribute a stabilizing yawing moment.

Finally a limited comparison has been made with the newly developed free wake lifting line code AWSM (van Garrel, 2003). The results for a positive yaw angle of 43 degrees are shown in the figures 10.6 and 10.7 together with the results from PHATAS. The obtained wake geometry is given in figure 10.5 and clearly shows skewness of the helical wake.
The trend of the AWSM result (which determines the yawing stability) at the 80% span location is more similar with the measurements than the PHATAS result. At the 30% section the differences are considerable. The explanation for these differences have not been found yet.

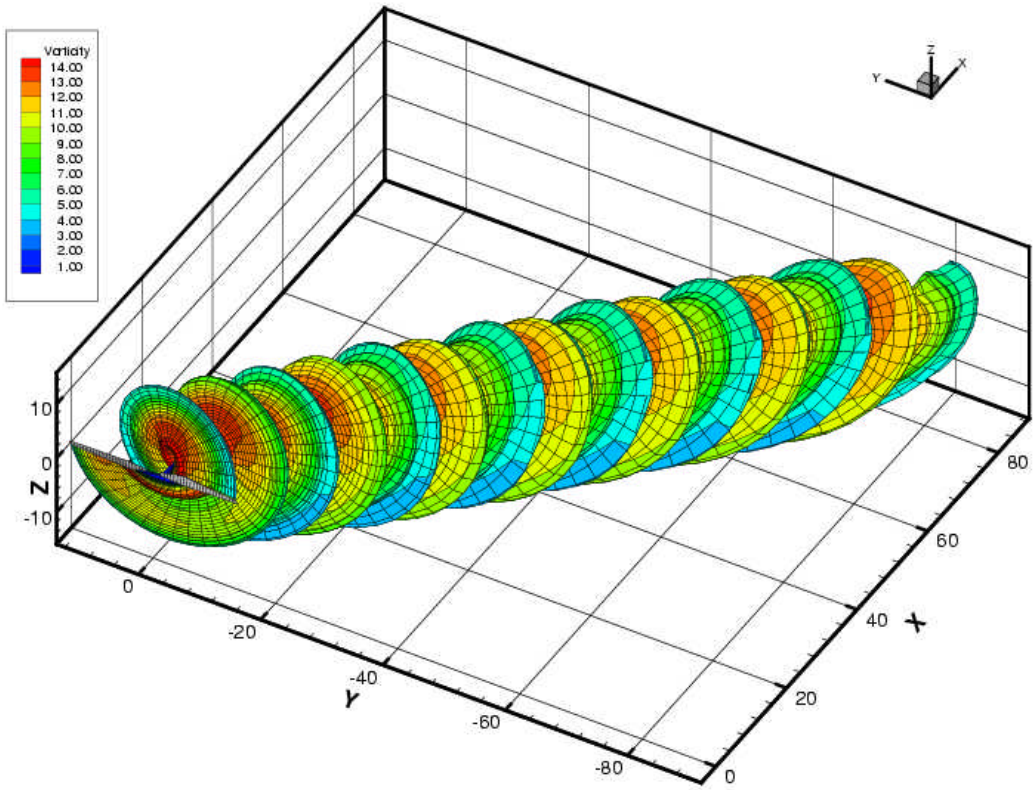

Figure 10.5: *Skewed Wake geometry calculated by AWSM*

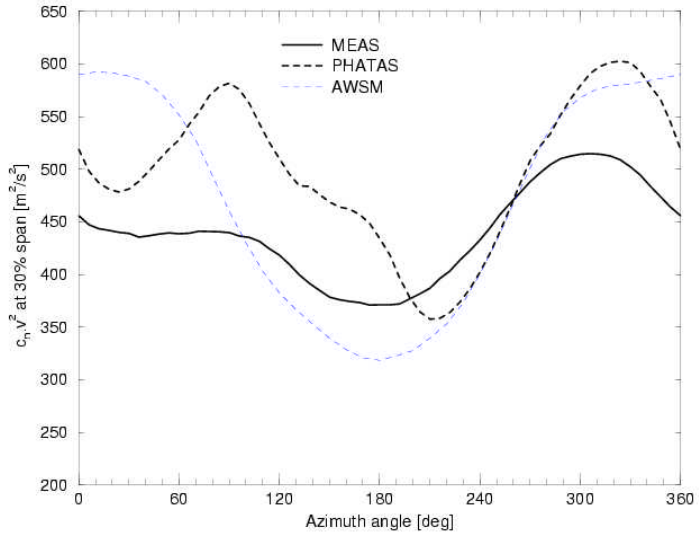

Figure 10.6: *ECN campaign: n-f_r at f_y = 42.9 deg and at a » 0.2; 30% span, calculated with PHATAS and AWSM*

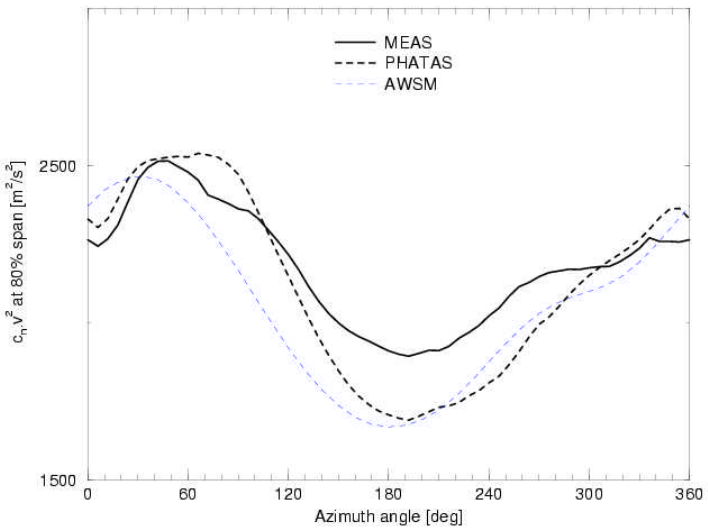

Figure 10.7 *ECN campaign: n-f_r at f_y = 42.9 deg and at a » 0.2; 80% span, calculated with PHATAS and AWSM*

11. Dissemination of results

In addition to the present final report of the Annexlyse project, the following task reports have been produced within the project (The reports can be found on the Internet site: http://www.ecn.nl/wind/other/annexlyse.html).

- Report of task 1 (Schepers, 2003b): "An inventory of analysis on the the IEA Annex XIV/XVIII database"
- Report of task 2 (van Rooij, 2004): "Definition of selection criteria for searching within the aerodynamic field test database"
- Report of task 3.1 (Lynn, 2003): "Angle of attack of a rotating wind turbine"
- Report of task 3.4 (Schepers, 2004b): "Annexlyse: Comparison between PHATAS calculations and IEA Annex XVIII measurements"
- Report of task 3.4 (Schepers, 2004d): "Annexlyse: Validation of yaw models on basis of detailed aerodynamic measurements on wind turbine blades"
- Report of task 4 (Schepers, 2004c): "Annexlyse: Improvement of aerodynamic models using IEA Annex XVIII measurements".

Furthermore 2 contributions have been submitted to the European Wind Energy Conference in Madrid in June 2003: (Schepers 2003a) "Detailed aerodynamic measurements: Analysis of results", and (van Rooij 2003b) "Validation of some stall models by analysis of IEA Annex XVIII field data".
The above mentioned task 3.4 and task 4 reports were summarized into a contribution to the EWEA special topic conference "The Science of Making Torque from the Wind", in Delft in April 2003 (see Schepers, 2004a). This contribution led to a publication in the Journal of Wind Energy (see Schepers, 2004e).
A thesis report has been made for the European Renewable Energy Master Program (EWEC) on a subject which was closely related to the Annexlyse project, see (Feigl 2003).

Finally the IEA Annex XVIII database on the Internet (http://www.ecn.nl/wind/other/IEA/index.en.html) has been updated within the Annexlyse project.

12. Conclusions

In the Annexlyse project a large number of investigations have been performed. The conclusions from each of these investigations will not be repeated here, but reference is made to the various Annexlyse reports, which are mentioned in section 11, i.e. (van Rooij, 2003a; van Rooij, 2003b; van Rooij 2005; Schepers, 2003a; Schepers 2004a; Schepers, 2004e).

The main conclusion from the Annexlyse project should be that, despite all measurement uncertainties, the character of the IEA Annex XIV/XVIII measurements is so much unique that they clearly contributed to the development and validation of aerodynamic models indeed. This holds among others for 3D stall models, tip models and yaw models. It was shown that the behaviour of blade and rotor loads can only be understood from measurements of the underlying sectional loads, as provided in this project. Thereto it should be realised that local aerodynamic effects like tip effects, rotational effects, the variation in induced velocity at yaw etc. were all shown to contribute significantly (in the order of 10% or more) to the overall blade and rotor loads. Additionally it was found that differences between calculated and measured blade and rotor loads (as found from conventional wind turbine validation programs, like the European Union JOULE III project Verification of European Wind Turbine Codes, (Schepers, 2001)) can have a very complicated origin and may even be caused by 'compensating errors'. Finally the fact that measurements on more than one wind turbine could be used, clearly led to a much more general validation of aerodynamic models where trends and dependencies on model parameters (i.e. blade layout, twist etc) could be confirmed, investigated and/or discovered.

13. References

Brand, A.J. (1994) *To estimate the angle of attack of an airfoil from the pressure distribution,* ECN-R--94-002 January 1994

Bruining, A. (1997) *Aerodynamic Characteristics of a 10m Diameter Rotating Wind Turbine Blade,* IW95-084R, Delft, September-1997

Bot, E.T.G. (2001) *Aerodynamische Tabel Generator*, ECN-C-01-077, August 2001

Chaviaropoulos, P.K. and Hansen, M.O.L. (2000): *Investigating 3D and rotational effects on wind turbine blades by means of a quasi-3D Navier Stokes Solver*, Journal of Fluids Engineering, Vol 122, No. 2, pp. 330-336, (2000).

Corten, G. (2001) *Flow Separation on wind turbine blades,* Dissertation University of Utrecht, 2001, ISBN 90-393-2582-0

Du, Z. and Selig, M. (1998): *A 3D stall delay model for horizontal axis wind turbine performance prediction*, Proceedings of the 1998 ASME Wind Energy Symposium, Reno, NV, Jan. 1998.

Feigl, L. (2003) *Analysis of aerodynamic field measurements on instrumented wind turbine rotors*, EUREC-Agency, Master Project, ECN, September, 2003

van Garrel, A. (2003) *Development of a wind turbine aerodynamics simulation module*, ECN, ECN-C--03-079, August, 2003

Kuik, G.A.M., van Rooij, R., Imamura M (2004) *Analysis of the UAE Phase VI wind turbine tunnel results in the non-yawed flow*,
Conference proceedings of EWEA, London (UK), November-2004

Lindenburg, C. and Hegberg, T. (1999) *PHATAS -- IV, User's manual*, ECN-C-99-093, 1999

Lindenburg, C. (2003) *Investigation into rotor blade aerodynamics, Analysis of the stationary measurements of the UEA Phase IV rotor in the NASA-Ames wind tunnel,*
ECN-C-03-025, June 2003

Lynn, M.J. (2003) *Angle of attack of a rotating wind turbine* Annexlyse Task 3.1 report, TU-Delft report, WE 04195, August 2003

van Rooij, R., Timmer, W.A. Bruining, A. (2002)
IJking van een stromingsrichtingprobe door windtunnelmetingen,
Annexlyse Task 3.1 report WE 02186, Delft, Maart 2002

van Rooij, R. (2003a) *Determination of the angle-of-attack for the test field experiments with RFOIL,* IEA Joint Action, Aerodynamics of Wind Turbines 16th Symposium, Boulder (USA), May-2003

van Rooij, R, Bruining, A. and Schepers, J.G. (2003b)
Validation of some rotor stall models by analysis of the IEA Annex XVIII field data,

Proceedings of EWEC European Wind Energy Conference Madrid, June 2003.

van Rooij R.P.J.O.M, and Schepers, J.G. (2004)
Definition of selection criteria for searching within the aerodynamic field-test database,
Annexlyse task 2 report, DUT-WE 04196, December 2004.

van Rooij, R., Schepers, J.G. (2005)
The Effect of Blade Geometry on the Normal Force Distribution of a Rotating Blade
AIAA conference, Reno (USA), Januari-2005

Schepers, J.G. and Snel, H. (1995), *JOULE2: Dynamic Inflow: Yawed Conditions and Partial Span Pitch,* ECN-C-95-056, June, 1995

Schepers, J.G. et al (1997),
Final report of IEA Annex XIV Field Rotor Aerodynamics ECN-C-97-027, June, 1997 http://www.ecn.nl/wind/other/IEA/index.en.html).

J.G. Schepers (1999) *An engineering model for yawed conditions developed on basis of wind turnnel measurements*', ASME Wind Energy Symposium, Reno USA", American Institute for Aeronautics and Astronautics", January 1999

Schepers, J.G. et al (2001),
Verification of European Wind Turbine Design Codes, VEWTDC, Final report ECN-C-01-053, December, 2001 http://www.ecn.nl/wind/other/vewtdc.html)

Schepers, J.G. et al (2002),
Final report of IEA Annex XVIII Enhanced Field Rotor Aerodynamics Database' ECN-C-02-016, February, 2002 http://www.ecn.nl/wind/other/IEA/index.en.html)

Schepers, J.G., van Rooij, R. and Bruining, A. (2003a)
Detailed aerodynamic measurements: Analysis of results
Proceedings of EWEC European Wind Energy Conference Madrid, June 2003.

Schepers, J.G., van Rooij, R. (2003b)
Annexlyse, Inventory of analyses on IEA Annex XIV/XVIII database
Annexlyse Task 1 report.

Schepers, J.G. et al (2004a)
Validation of aero-elastic codes, using detailed aerodynamic field measurements ,
Special Topic Conference 'The Science of making Torque from Wind", Session A6, April 2004

Schepers, J.G. and van Rooij, R. (2004b) *Annexlyse: Comparison between PHATAS calculations and IEA Annex XVIII measurements*, Annexlyse Task 3.4 report, August, 2004

Schepers, J.G. and Van Rooij, R. (2004c)
Annexlyse: Improvement of aerodynamic modelling using IEA Annex XVIII measurements,
Annexlyse Task 4 report, August 2004

Schepers, J.G. (2004d) *Annexlyse: Validation of yaw models on basis of detailed aerodynamic measurements on wind turbine blades*, Annexlyse Task 3.4 report, ECN-C-04-097, October 2004

Schepers, J.G. et al. (2004e) *Analysis of Detailed Aerodynamic Field Measurements using Results from an Aeroelastic Code* Journal of Wind Energy, Vol. 7, issue 4 pp.357-371, November 2004

W.Z. Shen, R. Mikkelsen, J.N. Sorensen and C. Bak (2003)
Tip loss corrections for wind turbine computations
AIAA Journal, 2003

Snel, H., Houwink R., and Bosschers J. (1993) *Sectional prediction of lift coefficients on rotating wind turbine blades in stall*, ECN-C--93-052, May 1993

Snel, H. and Schepers, J.G. (1994) *JOULE1: Joint investigation of Dynamic Inflow Effects and Implementation of an Engineering Method*, ECN-C-94-107, December 1994